2-1-2007

Neural and Electromyographic Correlates of Wrist Posture Control

Aaron J. Suminski
Marquette University

Stephen M. Rao
Cleveland Clinic

Kristine M. Mosier
Indiana University - Purdue University Indianapolis

Robert A. Scheidt
Marquette University, robert.scheidt@marquette.edu

Journal of Neurophysiology, Vol. 97, No. 2 (February 2007): 1527-1545. DOI.

Neural and Electromyographic Correlates of Wrist Posture Control

Aaron J. Suminski
Department of Biomedical Engineering, Marquette University, Milwaukee, Wisconsin
Stephen M. Rao
Department of Neurology, Medical College of Wisconsin, Milwaukee, Wisconsin
Kristine M. Mosier
Department of Radiology, Indiana University School of Medicine, Indianapolis, Indiana
Robert A. Scheidt
Department of Biomedical Engineering, Marquette University, Milwaukee, WI
Department of Physical Medicine and Rehabilitation, Feinberg School of Medicine, Northwestern University, Chicago, Illinois

Abstract

In identical experiments in and out of a MR scanner, we recorded functional magnetic resonance imaging and electromyographic correlates of wrist stabilization against constant and time-varying mechanical perturbations.

Positioning errors were greatest while stabilizing random torques. Wrist muscle activity lagged changes in joint angular velocity at latencies suggesting *trans*-cortical reflex action. Drift in stabilized hand positions gave rise to frequent, accurately directed, corrective movements, suggesting that the brain maintains separate representations of desired wrist angle for feedback control of posture and the generation of discrete corrections. Two patterns of neural activity were evident in the blood-oxygenation-level-dependent (BOLD) time series obtained during stabilization. A cerebello-thalamo-cortical network showed significant activity whenever position errors were present. Here, changes in activation correlated with moment-by-moment changes in position errors (not force), implicating this network in the feedback control of hand position. A second network, showing elevated activity during stabilization whether errors were present or not, included prefrontal cortex, rostral dorsal premotor and supplementary motor area cortices, and inferior aspects of parietal cortex. BOLD activation in some of these regions correlated with positioning errors integrated over a longer time-frame consistent with optimization of feedback performance via adjustment of the behavioral goal (feedback setpoint) and the planning and execution of internally generated motor actions. The finding that nonoverlapping networks demonstrate differential sensitivity to kinematic performance errors over different time scales supports the hypothesis that in stabilizing the hand, the brain recruits distinct neural systems for feedback control of limb position and for evaluation/adjustment of controller parameters in response to persistent errors.

INTRODUCTION

Tool use is an important aspect of human development, and meaningful interaction with our environment frequently requires both the stabilization of hand-held objects about desired limb postures and the movement of such objects between stable postures. Recent experimental evidence suggests that distinct neural mechanisms may be involved in the planning and control of simple motor actions such as reaching with the arm and stabilizing it against environmental loads (Kurtzer et al. 2005; Lackner and Dizio 1994; Scheidt et al. 2004). The neural mechanisms subserving reaching and trajectory control have received a great deal of recent attention, whereas study of the central mechanisms supporting final position control and its optimization within a given task context have received much less attention. Here we describe a set of experiments using a novel, MR-compatible robot designed to examine both the central and peripheral mechanisms contributing to the control of wrist posture.

When the position of a limb is actively maintained, unexpected changes in the load elicit a series of changes in muscle activity (Evarts and Tanji 1976; Evarts and Vaughn 1978; Lee and Tatton 1975; Marsden et al. 1978) termed the M1, M2, and M3 responses (Lee and Tatton 1975). The M1 component has the shortest latency occurring ~25 ms after a perturbation and is caused by the monosynaptic (segmental) reflex response to muscle stretch. It is followed in time by the M2 and M3 responses, which occur at latencies between 40 and 100 ms. Single-unit recordings in primates demonstrate that these “long loop” reflex pathways are mediated by supraspinal pathways including neural populations in both the primary sensorimotor cortex (Evarts and Tanji 1976; Thach 1978) and the cerebellum (Strick 1978, 1983; Thach 1978). These neuromuscular responses are important in the compensation for unexpected perturbations because both the segmental (Sinkjaer and Hayashi 1989) and the transcortical “reflex” responses (Evarts and Fromm 1981; Evarts and Tanji 1976; Miall et al. 1993; Strick 1978) have been implicated in the moment-by-moment (closed-loop or “on-line”) feedback control of joint position.

However, subjects may invoke alternative strategies to maintain the position of the limb. These strategies include impedance control via voluntary co-activation of antagonist muscles about the joints (i.e., cocontraction), whereby intrinsic muscle mechanical properties provide an immediate mechanical response to the perturbation (Loeb et al. 1999; Nichols and Houk 1976), or they can also generate discrete, feedforward, corrective movements compensating for the approximate mean of the perturbation (Fagg et al. 1998; Haaland

and Harrington 1989). These strategies are not mutually exclusive but rather are complementary in two ways. First, they act to reduce performance errors over different timescales (ranging from the short-latency mechanical responses of antagonist co-activation and reflex action to the reduction of persistent errors by discrete adjustment of behavioral goals). Second, they provide the flexibility in motor output needed to respond to task-dependent constraints on accuracy and muscular effort and thus may provide the behavioral basis for optimality in human motor control (Scott 2004; Todorov and Jordan 2002). That is, by monitoring long-term trends in task-relevant variables, an optimal neural controller can adjust feedback parameters (including the feedback control setpoint) to optimize those aspects of motor output of greatest importance given the task at hand (Scott 2004). Much is yet unknown about the neural mechanisms mediating wrist position control (i.e., posture stabilization), including what aspects of environmental perturbation are compensated on a moment-by-moment basis in this task (hand force, position, or both) and what performance variables might cause subjects to invoke a discrete corrective action during stabilization.

Functional imaging techniques provide a valuable tool for studying the central neural networks contributing to motor behavior in humans. The majority of functional magnetic resonance imaging (fMRI) studies of motor behavior have heretofore been unable to probe the mechanisms involved in the control of limb position due to the lack of devices available to perturb human movement in a controlled manner within the MR environment. Instead, research has focused on eye-hand coordination (Miall et al. 2000, 2001), visuomotor adaptation (Flament et al. 1996; Imamizu et al. 2000), force control (Dai et al. 2001; Ehrsson et al. 2001; Thickbroom et al. 1998; Vaillancourt et al. 2003), and the feedforward and feedback control of joystick-mediated cursor movement (Seidler et al. 2004). Notable exceptions include studies by Shadmehr and colleagues, who have used both PET and fMRI to study the neural correlates of motor learning (Nezafat et al. 2001), memory consolidation (Shadmehr and Holcomb 1997), and trajectory errors (Diedrichsen et al. 2005) as subjects performed reaching movements while holding the handle of a two-joint robot. Similarly, Desmurget and colleagues used PET to investigate the neural mechanisms related to the correction of movement trajectories during a pointing task (Desmurget et al. 2001). But given that limb trajectory and final position control might be served by distinct neural mechanisms (Ghez et al. 2004; Kurtzer et al. 2005; Scheidt et al. 2004), a design limitation of those studies is that the tasks and neural imaging techniques used were not well-suited for decoupling the control of trajectory from final posture due to the long integration periods associated with the hemodynamic and metabolic dynamics associated with fMRI and PET. Thus there is a need to reevaluate whether limb stabilization excites neural pathways during feedback control of position which are anatomically and functionally distinct from those involved in the generation of discrete compensatory responses.

Here we describe experiments designed to investigate the central and peripheral mechanisms contributing to the control of wrist position using fMRI and electromyography (EMG), respectively. Subjects grasped the handle of a novel MR-compatible robot both in and out of a MR scanner and stabilized their right hand against constant (CT) and random (RT) extensor torque perturbations having the same mean value. Stabilization was preceded and followed by brief periods of passive manipulation of the hand during which subjects were instructed to relax. Vision of the wrist was precluded at all times, forcing subjects to rely strictly on proprioceptive feedback during stabilization. We anticipated that EMG would demonstrate that the two wrist extensor loads elicit different combinations of compensatory responses throughout the stabilization period, promoting feedback control of limb position regardless of load (evidenced by the recruitment of long-loop reflexes), while encouraging an increase in limb impedance when the load was uncertain. We also thought it possible that subjects might adjust their behavioral goals by generating discrete, feedforward, corrective movements if ongoing feedback control failed to meet subjective accuracy requirements. We therefore hypothesized that at least two, distinct, neural mechanisms contribute to the stabilization of wrist position in the presence of persistent environmental perturbations. A first mechanism likely mediates the on-line control of endpoint position (not torque) via feedback control. Because feedback control attempts to adjust motor commands to

cancel deviations of the limb from its desired state, regions contributing to feedback control of wrist position will likely show increased blood-oxygen-level-dependent (BOLD) response during periods wherein limb positioning errors are present independent of the level of force generated (i.e., throughout RT stabilization as well as during the passive movements that occurred before and after stabilization). Ideally, temporal variations in the BOLD response in these regions should correlate with variations in wrist position on a moment-by-moment basis. A second mechanism likely monitors performance over a longer timeframe than the feedback mechanisms, generating discrete, conditional, corrective actions when feedback control fails to eliminate persistent errors. Regions contributing to this higher-order evaluation of performance are expected to show increased BOLD response during both RT and CT stabilization regardless of whether positioning errors are present as well as variations in BOLD response that reflect changes in positioning errors with a longer temporal integration period. Consistent with these expectations, the data suggest that when stabilizing the hand against environmental perturbations, subjects recruit distinct brain networks for the ongoing regulation of limb position (i.e., feedback control) and for the evaluation of feedback control and the feed-forward planning and execution of internally generated corrective actions.

METHODS

Ten healthy volunteers participated in each of the two sessions of this study (5 female; mean age = 27.5 yr, range = 21–38). All subjects were right-handed according to the Edinburgh Handedness Inventory (Oldfield 1971). Subjects were excluded if they had significant neurological, psychiatric, or other medical history or were taking psychoactive medications. Additional exclusion criteria were specific to MR scanning: pregnancy, weight inappropriate for height, ferrous objects within the body, low visual acuity, and a history of claustrophobia. Written informed consent was obtained from each subject in accordance with institutional guidelines approved by the Medical College of Wisconsin and Marquette University in accord with the Declaration of Helsinki.

Description of robotic tool

A MR-compatible manipulandum with integrated pneumatic actuator was developed to exert computer controlled torques about the subject's right wrist (Fig. 1*A*). The device monitors wrist position (within 0.05°) and wrist torque (within 0.001 Nm). Air pressure within the actuator is sensed by a Honeywell 26PC series pressure transducer (Honeywell International, Morristown, NJ), and digitized with a National Instruments PCI-6036E multifunction data-acquisition system (National Instruments, Austin, TX). Analog measurements of pressure within the actuator are amplified and Nyquist filtered at a cutoff frequency of 20 Hz. Joint angle is measured with an Agilent HEDM-6540, 3-channel, Mylar film optical encoder (Agilent Technologies, Palo Alto, CA), paired with a Measurement Computing PCI-QUAD-04 incremental encoder driver (Measurement Computing, Middleboro, MA). Robot control is achieved using custom hardware and software designed to use the XPC target, real-time operating system (Mathworks, Natick, MA). Wrist angle and actuator pressure data were acquired at the control loop rate of 1,000 Hz. Experiments demonstrating the compatibility of the robot and MR scanner are presented in appendix a.

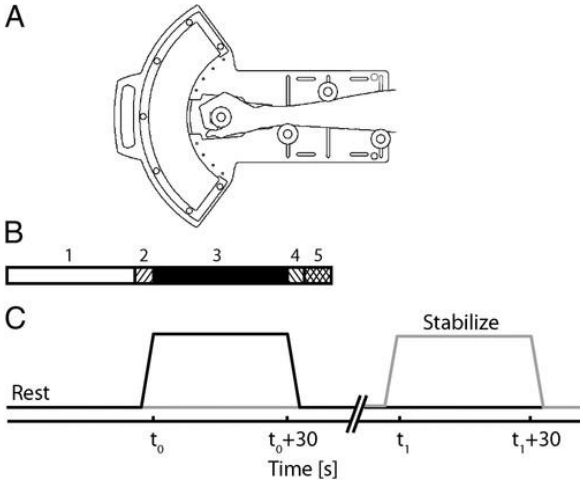

FIG. 1.*A*: schematic representation of the 1 degree of freedom pneumatic manipulandum illustrating how the subject interfaces to the device. *B*: a single trial was conducted in 5 phases. During the 30 s prior to stabilization (phase 1), the subject was instructed to relax while the robot held the hand in a comfortable posture of 40° flexion. Three seconds prior to the start of stabilization (phase 2), the robot moved the relaxed hand to the target posture (20° flexion) and held it there until the onset of the stabilization period. During stabilization periods (phase 3), subjects were instructed to hold their wrist steady at a comfortable target angle of 20° flexion. At the end of the stabilization period, the subject was instructed to relax, and the robot again moved the passive hand to its resting position at 40° flexion (phase 4) after which resting electromyograms (EMG) were monitored for 3 s (phase 5). *C*: subjects performed the wrist-stabilization task in a blocked design experiment that alternated between periods of rest and active stabilization. During phase 3, subjects stabilized against either constant (gray line) or pseudo-random (black line) extensor torque perturbations. Each of the 2 trial types was presented 1 time in pseudorandom order during a run (e.g., subjects could not predict the perturbation on the next trial), along with 30-s periods of inactivity (rest) preceding and following each stabilization period.

Experimental procedures

Subjects participated in two experimental sessions designed to evaluate the electromyographic and neural correlates of wrist stabilization. To allow for the collection of EMG data from task-relevant muscles, subjects performed the experiment while inside a mock MR scanner located at Froedert Memorial Lutheran Hospital in Milwaukee, WI. Each subject also performed the identical stabilization experiment in a separate session while simultaneously undergoing fMRI scanning in a 1.5T General Electric Signa scanner (General Electric Healthcare, Milwaukee, WI) equipped with a three-axis local gradient head coil and an elliptical endcapped quadrature radiofrequency coil at Froedert.

In both sessions, subjects rested supine in the scanner with their head constrained by foam padding to reduce head motion inside the head coil. With arms at their sides, subjects grasped the robot handle with their dominant hand. The handle's axis of rotation was aligned with that of the wrist, and the frame of the device was secured to both the subject's forearm and the inner wall of the scanner bore for support. A single trial was conducted in 5 phases (Fig. 1*B*). During the 30 s prior to stabilization (phase 1), the subject was instructed to relax while the robot held the hand in a comfortable resting posture of 40° flexion (θ_r). Three seconds prior to the start of stabilization (phase 2), the robot moved the relaxed hand to the target posture (20° flexion) and held it there until the onset of the stabilization period. The purpose of this phase was to provide subjects a salient haptic cue of the desired wrist angle about which they were to stabilize. During the 30 s stabilization periods (phase 3), subjects were instructed to hold their wrist steady at the target angle during two experimental conditions in which the device was programmed to apply either a predictable, constant extensor torque about

the wrist (CT, mean = 1.2 Nm) or unpredictable, pseudo-random extensor torques composed of band-limited Gaussian “white” noise with a high-frequency cutoff of 1.6 Hz (RT; 1.2 ± 1.1 Nm; mean ± SD both here and elsewhere). At the end of the stabilization period, the subject was instructed to relax, and the robot again moved the passive hand to its resting position at 40° flexion (phase 4) after which resting EMG continued to be monitored for 3 s (phase 5). Direct view of the wrist was precluded and subjects received no visual feedback of hand motion during stabilization phase 3. Instead subjects were provided with a stationary visual fixation target that was visible using prism glasses and was back-projected onto a screen located at their feet. The fixation target moved in concert with the hand during passive movement phases 2 and 4 and thus provided an implicit visual representation of the desired wrist angle during stabilization phase 3. Subjects received experimental instructions between trials via the back-projection screen.

Both sessions consisted of a blocked design experiment that alternated between periods of rest and active stabilization. Each of the two trial types was presented one time in pseudo-random order during a run, along with 30-s periods of inactivity (rest) preceding and following each stabilization period (Fig. 1*C*). Thus there were 60 s of rest between stabilization periods within each run to minimize the occurrence of fatigue. Each subject performed 10 of these runs in each session. During actual imaging runs, whole-brain images were acquired using a single-shot, blipped gradient-echo echo-planar pulse sequence (19 contiguous sagittal 7-mm slices, TE = 40 ms, TR = 2.5 s, 90° flip angle, FOV = 24 cm, 64 × 64 matrix, 3.75-mm in-plane resolution); 72 whole-brain images were acquired in each run. BOLD contrast was used to image the hemodynamic related changes in the brain occurring during the two stabilization tasks. Before functional imaging, high-resolution three-dimensional (3D) spoiled gradient recalled at steady-state T1-weighted anatomic images were collected for anatomic localization and co-registration (TE = 5 ms, TR = 24 ms, 40° flip angle, slice thickness = 1.2 mm, FOV = 24 cm, 256 × 192 matrix).

EMG data collection and analysis

In the mock scanning session, EMGs were recorded from 10 wrist and arm muscles using differential surface electrodes while subjects stabilized their wrists (Delsys DE-2.1 electrodes and Delsys Bagnolli 16 system; Delsys, Taunton, MA). Monitored muscles included: wrist and finger flexors and extensors (flexor carpi radialis, FCR; flexor carpi ulnaris, FCU; flexor digitorum superficialis, FDS; extensor carpi radials, ECR; extensor carpi ulnaris, ECU; and extensor digitorum communus, EDC), an elbow flexor and extensor (the short head of biceps, BIC; and lateral head of triceps, TRI), and a shoulder flexor and extensor (anterior deltoid, AD; and posterior deltoid, PD). EMG signals were band-pass filtered between 10 and 450 Hz, amplified (×1000), and sampled at 1,000 Hz using a National Instruments PCI-6036E multifunction data acquisition system (National Instruments). Residual offsets were subsequently removed from the digitized EMGs, which were then rectified and filtered at 4 Hz with a zero-phase low-pass filter (4^{th}-order Butterworth). To allow for comparison of EMG activity across the study population, each subject's muscle activities were subsequently normalized by the peak value of the rectified and filtered activity recorded from that muscle during a series of maximum voluntary isometric contractions (MVIC). Each subject performed a total of 12 MVIC trials prior to the start of the stabilization experiment: two each of maximal isometric wrist flexion, wrist extension, elbow flexion, elbow extension, shoulder flexion, and shoulder extension. The peak magnitude of EMG activity for each muscle was defined as the largest value of EMG after signal processing as described in the preceding text.

The resulting normalized EMG time series were averaged across trials within each trial type for each subject to obtain an estimate of each muscle's activity during both CT and RT stabilization. We used a cross-correlation technique (Neilson 1972) to evaluate the temporal relationship between changes in wrist joint angle ($d\theta/dt$) and individual muscle activities during stabilization. Significance was evaluated by comparing the correlation magnitude to an estimate of the 95% confidence interval bounding zero correlation (Box et al. 1994). We then characterized the coordination between muscles at each joint by estimating the degree of antagonist muscle co-

activity (CoA) at the wrist, elbow, and shoulder joints using a measure also known as “wasted contraction” (Thoroughman and Shadmehr 1999). We considered the AD and PD as shoulder antagonists, BIC and TRI as elbow antagonists, and the FCR and ECR muscles as wrist antagonists. For each pair of antagonist muscles and at each sampling instant, the minimum value of the two normalized EMG signals was selected to yield a time varying co-activity signal which represents the magnitude of normalized EMG that is equal and opposite in the antagonist muscle pair

$$\mathrm{CoA(nT)} = \min\left(\mathrm{E\bar{M}G}^{\mathrm{norm}}_{\mathrm{flexor}}(\mathrm{nT}), \mathrm{E\bar{M}G}^{\mathrm{norm}}_{\mathrm{extensor}}(\mathrm{nT})\right)$$

(1)

Finally, we computed for each subject and for each muscle at each joint, the amount of EMG activity exceeding the co-activity value computed for that joint. This value, which we call the excess-activity (ExA), estimates the amount of EMG above and beyond that which contributes to coactivation about the joint, roughly estimating the amount (magnitude) of phasic muscle activity that may contribute to moment-by-moment feedback compensation for the imposed loads

$$\mathrm{ExA(nT)} - \mathrm{E\bar{M}G}^{\mathrm{norm}}(\mathrm{nT}) - \mathrm{CoA(nT)}$$

(2)

Behavioral data analysis

Time series of joint angle and joint angular velocity were low-pass filtered at a cutoff frequency of 10 Hz to reduce encoder state transition artifacts. Stabilization was evaluated using five kinematic and one dynamic performance measures. First, we computed *objective stabilization error* ε_o(nT) as the difference between the actual and desired (target) hand position

$$\varepsilon_{\mathrm{o}}(\mathrm{nT}) = \theta(\mathrm{nT}) - \theta_t$$

(3)

where θ_t is the target wrist angle (20° flexion) and θ(nT) is the instantaneous wrist angle at sample instant nT. To compare objective performance across stabilization conditions, we then computed the root mean square (RMS) value of this time series throughout each 30-s trial

$$\mathrm{RMS}_{\mathrm{TRIAL}}\varepsilon_{\mathrm{o}} = \sqrt{\frac{1}{N}\sum_{n=1}^{N}\left(\varepsilon_{\mathrm{o}}(\mathrm{nT})\right)^2}$$

(4)

where *N* is the total number of data samples during each stabilization period (i.e., 30,000).

We next quantified *drift* in the instantaneous joint angle equilibrium position by fitting a first-order polynomial to the joint angle time series data over the final 20 s of each trial. Drift was considered significant in those trials where the slope of the regression line was statistically different from zero. This polynomial defined the subjective target angle θ_s(nT) as the instantaneous reference angle about which small corrections were made, and was used to estimate *subjective stabilization error* ε_s(nT) as the RMS deviations about θ_s(nT)

$$\varepsilon_{\mathrm{s}}(\mathrm{nT}) = \theta(\mathrm{nT}) - \theta_{\mathrm{s}}(\mathrm{nT})$$

(5)

For comparing subjective performance across stabilization conditions, we computed its RMS throughout each 30-s trial

$$\mathrm{RMS}_{\mathrm{TRIAL}}\varepsilon_{\mathrm{s}} = \sqrt{\frac{1}{N}\sum_{n=1}^{N}\left(\varepsilon_{\mathrm{s}}(\mathrm{nT})\right)^{2}}$$

(6)

where again, *N* is the total number of data samples during stabilization (30,000).

We also identified the onset and direction of *discrete corrective movements* made by subjects during both RT and CT stabilization (Fig. 3*A*, *top*). Here we wished to identify relatively rapid movements that were not a direct mechanical consequence of moment-by-moment fluctuations in wrist torque generated to oppose the perturbation. Thus for each stabilization condition for each individual subject, we removed the trial-averaged wrist angle trajectory from every individual trial to obtain a "corrected" wrist angle time series (θ_C, Fig. 3*A*, *middle*). We considered as discrete corrections only those movements wherein the angular velocity of corrected wrist angle trajectories ($d\theta_C/dt$) exceeded 5°/s, occurring ≥1 s after the start of a stabilization period (Fig. 3*A*, *bottom*). Both the total number of trials where at least one discrete corrective movement was detected and the total number of discrete movements across all trials were counted. In addition, we classified each correction movement as being correctly or incorrectly directed based on the relationship of the wrist angle and the objective target position θ_t at the instant angular velocities exceeded the threshold.

We then constructed an estimate of *state estimation errors* ε_q(nT) during phases 2–4 of each trial (i.e., during stabilization as well as during the preceding and following passive movement phases). Here we assume that during trial phases 2 and 4, passive movement of the wrist induced a discrepancy between actual limb position and that expected given the recent history of motor output, whereas during trial phase 3, state estimation errors would arise from load-induced deviations from the subjective target angle θ_s(nT). Specifically

$$\varepsilon_{\mathrm{q}}(\mathrm{nT}) = \begin{cases} \theta(\mathrm{nT}) = \theta_{\mathrm{r}} & \text{phase 2} \\ \varepsilon_s(\mathrm{nT}) & \text{phase 3} \\ \theta(\mathrm{nT}) = \theta_{\mathrm{t}} & \text{phase 4} \end{cases}$$

(7)

The time series of ε_q(nT) were then used to compute RMS values of state estimation errors on a moment-by-moment basis (i.e., within a 2.5-s integration window emulating the temporal sampling of the functional imaging pulse sequence, TR)

$$\mathrm{RMS}_{\mathrm{TR}}\left(\varepsilon_{\mathrm{q}}(\mathrm{mN})\right) = \frac{1}{N}\sum_{\mathrm{n}=1}^{N}\left(\varepsilon_{\mathrm{q}}(\mathrm{nT}+\mathrm{mN})\right)^{2}$$

(8)

where m is the total number of TR sampling instants during phases 2–4 of the trial and *N* is the number of wrist angle sampling instants in each TR integration period (i.e., 2,500).

Finally, we computed RMS *wrist torque* values, again on a moment-by-moment basis (i.e., within a 2.5-s integration window as in *Eq. 8*) and on a trial-by-trial basis (during phase 3 as in *Eq. 6*). Because wrist angular deviations about the desired target angle were small, torque values were estimated to be proportional to the transduced actuator pressure.

fMRI data analysis

Functional MR images were generated and analyzed within the Analysis of Functional NeuroImages (AFNI) software package (Cox 1996). The three images at the beginning and ending of each run were discarded to allow for equilibration of the magnetic field. For each subject, individual run image time series were concatenated into one large dataset and then aligned in three-dimensional space to minimize the effects of head motion; an interactive, linear, least-squares method was used for this purpose (AFNI program 3dVolreg) (Cox 1996). Registration yielded six movement indices per functional imaging run. The across-subjects average head movement for each of the rotation indices were 0.23 ± 0.12, 0.19 ± 0.24, and 0.35 ± 0.34° (rotations in the superior-inferior, anterior-posterior, and left-right planes, respectively), whereas average translational head movement was 0.40 ± 0.29, 0.24 ± 0.31, and 0.28 ± 0.24 mm (translation in the superior-inferior, anterior-posterior, and left-right direction). No subjects were excluded from further analysis due to head motion. A voxel-wise multiple linear regression analysis was used to determine the amount of fMRI signal contrast between the two task conditions (stabilization against constant CT or random RT torques), and the resting baseline. The two input reference functions consisted of a time series (having the value 1 during each stabilization period of a given stimulus type and 0 otherwise) convolved with a γ-variate function to model the dynamics of the hemodynamic response. A second multiple regression analysis was performed to determine the amount of fMRI signal contrast between the two task conditions and the resting baseline, but only during the middle third of stabilization trials (that is, RT_M and CT_M). This analysis focuses on activation patterns during stabilization itself disregarding activations due to transient events at the beginning and end of trial phase 3. In both regression analyses, the time series of head motion indices (obtained from the spatial registration process) were included in the model of resting baseline to reduce the potential for false positives due to stimulus correlated motion.

The resulting functional images for RT, CT, RT_M, and CT_M were interpolated to obtain a volumetric grid having 1-mm^3 voxel volumes, coregistered, and then converted into the Talairach stereotaxic coordinate space (Talairach and Tournoux 1988). To facilitate group analysis, the Talairached functional images were spatially blurred using a 4-mm Gaussian full-width half-maximum filter to compensate for inter-subject anatomical variability. *T*-tests were performed on a voxel-wise basis on the regression fit coefficients for RT, CT, RT_M, and CT_M to identify regions showing greater activation during stabilization as compared with rest. In addition, a mixed-model ANOVA with post hoc *t*-tests (treating subjects as a random factor) was used to identify regions showing differences in level of activation between the RT and CT conditions. In all across-subject analyses, a cluster-size and thresholding technique was used to correct for multiple comparisons in the group analysis. Appropriate cluster size (554 μl, 5.6 voxels) and individual voxel *P* value thresholds ($P = 0.005$) were estimated by performing 5,000 iterations in a Monte-Carlo simulation using the AlphaSim tool included within the AFNI toolkit (Cox 1996). The location of activated regions in group statistical parametric maps was obtained using the Talairach atlas (Talairach and Tournoux 1988) for cerebral activations and the Schmahmann atlas (Schmahmann 2000) for activations in the cerebellum and its nuclei. Cortical activations were visualized using CARET (Van Essen et al. 2001) (http://brainmap.wustl.edu/caret).

To evaluate the pattern of neural activity due to stabilization, we extracted for each individual subject the average BOLD time series from each of 18 ROIs in which significant activation was observed in either RT or CT relative to rest (see Table 1). We then computed the percentage BOLD signal change (PSC) relative to a local baseline as a function of time for both RT and CT trials. For this calculation, the local baseline was defined by

fitting a first-order polynomial through data from the two 30-s rest periods immediately preceding and after each stabilization period for each individual subject and ROI. PSC time series for the population were created by averaging individual RT and CT time series within ROI and across subjects.

TABLE 1. *Brain regions exhibiting significant task-related activation during RT or CT trials*

		Talairach Coordinates				
	Hemisphere	*X*	*Y*	*Z*	Volume, $\mu 1$	Mean *T*
Cluster 1						
Precentral gyrus (BA 4,6) Postcentral gyrus (BA 2,3)	L	-30.1	-19.4	51.3	14166	5.884
Medial frontal gyrus (BA 6) Cingulate gyrus (BA 24,31)	B	-0.5	-11.6	48	7856	5.0334
Inferior/superior parietal lobule (BA 5,7,40)	L	-30.3	-38.3	56.6	2530	4.7958
Precentral gyrus (BA 6)	R	49.6	-2.4	39	957	4.5238
Precentral gyrus (BA 6)	R	22.3	-15.4	61.2	866	4.2839
Middle temporal gyrus (BA 39)	R	52.6	-68.9	15.9	596	4.3556
Cluster 2						
Cortica						
Insula (BA 13) Superior temporal gyrus (BA 22,41) Precentral gyrus (BA 6)	L	-47.5	0.2	8.3	8102	4.8657
Inferior parietal lobule (BA 40)	L	-50.9	31.5	24.9	7477	4.9995
Insula (BA 13) Superior temporal gyrus (BA 22)	R	42.7	5.6	4.8	5633	5.0229
Inferior parietal lobule (BA 40) Supramarginal gyrus	R	53.4	-40.6	36.4	5125	4.3849
Middle/inferior frontal gyrus (BA 10,46)	R	39.2	38.5	3.5	2668	4.5259
Middle/inferior frontal gyrus (BA 10,45,46) Claustrum	L	-42	29.8	12.5	1334	4.3385
Inferior parietal lobule (BA 40) Angular gyrus	L	-49.1	-53.3	39.9	1079	4.1923
Medial frontal gyrus (BA 6.8) Cingulate gyrus (BA 32) Superior frontal gyrus (BA 8)	B	-3	25.4	41.5	1033	4.156
Superior frontal gyrus (BA 6)	R	22.1	13.3	51.6	687	4.5912
Middle frontal gyrus (BA 10)	L	-38.2	49.2	3.4	582	4.2741
Subcortical						
Cerebellar cortex lobule IV, V, VI Vermis	B	5.9	-49.4	-14	9571	5.2885
Dentate	B					

Basal ganglia and thalamus Putamen Globus pallidus (medial/lateral) Caudate (body, tail) Ventral lateral Ventral posterior medial/lateral Medial dorsal Ventral anterior Lateral posterior Pulvinar	L	-19.7	-17	10.1	6684	5.025

L, left; R, right; B, bilateral; BA = Broadman's Area.

On visual examination of the PSC time series for each ROI and each trial type, two distinctive patterns (or features) of the time series became evident. First, some ROIs demonstrated great sensitivity to load type and considerable sensitivity to passive movement of the wrist during trial phases 2 and 4. Second, some ROIs demonstrated elevated activity during stabilization against both load types and no sensitivity to passive motion of the wrist. Finally, some ROIs demonstrated some characteristics of each of the two patterns. To quantify these observations, we defined a two-element feature vector $\Psi = \{\bar{S}, \Delta_M\}$ summarizing the average increase in PSC induced by passive movement in phase 2 ($\bar{S}$) and the difference in PSC between RT and CT trials during stabilization (Δ_M). The $\bar{S}$ feature was the average of four consecutive TR samples from each of the RT and CT trials, beginning two points (i.e., 2 TR) prior to the start of the stabilization period. The Δ_M feature was computed as the difference between the average RT and CT PSC time series during the middle 20-s (8 TR) of stabilization. We then classified each ROI into one of two clusters based on similarity of BOLD PSC activation captured by Ψ using a k-means clustering technique (Johnson and Wichern 2002) within the Minitab 14 statistical computing environment (Minitab, College Park, PA). K-means clustering is a nonheirarchical clustering technique used to classify data into K groups when the groups are initially unknown. Data were assigned to a cluster by minimizing the Euclidain distance within the feature space between the data and corresponding cluster centroids, which are initialized a priori but are allowed to adapt. Values of Ψ extracted from the primary sensorimotor cortex and presupplementary motor area (pre-SMA)/rostral cingulate zone (RCZ) ROIs were used to define the initial value of the centroids of the clusters. Results of the cluster analysis were insensitive to the particular seed regions selected initially.

Because stability of control requires that parametric adjustment of an optimal feedback controller progress more slowly than error compensation provided by the controller itself (cf. Widrow and Walach 1996), we performed a final set of BOLD correlation analyses designed to identify brain regions explicitly involved in the moment-by-moment and long-term correction for kinematic and/or kinetic performance errors. Here, we performed four separate AFNI regression analyses using input reference functions corresponding to the magnitude of $RMS_{TR}(\varepsilon_q(mN))$, $RMS_{TRIAL}(\varepsilon_o)$, and RMS torque both on a trial-by-trial and TR-by-TR basis ($Error_{Trial}$, $Error_{TR}$, $Torque_{Trial}$, and $Torque_{TR}$). Each input reference function was created from error or pressure data measured during the corresponding stabilization run within the MR-scanner. The value at each (TR) sampling instant for reference functions that varied on a trial-by-trial basis was set equal to the RMS error (torque) value computed throughout the corresponding stabilization period (30-s integration window). The value at each (TR) sampling instant for reference functions that varied on a moment-by-moment basis was set equal to the RMS error (torque) value computed during that TR sampling period (2.5-s integration window). In all cases, the input reference time series were convolved with a γ-variate function to model the temporal filtering properties of the hemodynamic response. Additional reference time series separately identifying periods of RT and CT

stabilization were included in each AFNI regression analysis to account for the average activation due to stabilization within each task. Again, time series of head motion indices were included in the model of resting baseline to reduce the potential for false positives due to stimulus correlated motion. The resulting functional images were interpolated, co-registered, warped into a sterotactic coordinate frame, and blurred to facilitate between subject analyses as described above. Voxelwise, one-sided *t*-tests were used to identify regions where activation was significantly modulated by $Error_{Trial}$, $Error_{TR}$, $Torque_{Trial}$, or $Torque_{TR}$. In each case, we restricted our search to regions identified as being active during stabilization against either RT or **CT** perturbations (Fig. 5*A*), thus applying a reduced cluster size threshold of 262 µl (2.6 voxels) and individual voxel statistical threshold of $P = 0.005$ to correct for multiple comparisons in the AFNI statistical analyses.

Statistical testing of behavioral and EMG performance measures

Objective RMS stabilization errors were averaged within subject by trial type. Planned, paired *t*-tests were used to test the null hypothesis that the mean RMS errors from the two stabilization conditions were equal ($\varepsilon_{CT} - \varepsilon_{RT} = 0$) in both the MRI and mock-MRI experimental sessions. Next for each subject and each load condition, we averaged the objective RMS stabilization errors from the first two trials, the second pair of trials, on up to the last pair of trials (*trials 9* and *10*) to yield five average RMS error scores. We then used separate, repeated-measures ANOVA for the RT and CT tasks to determine whether task performance improved throughout the experimental sessions. At the wrist, planned, paired *t*-tests were used to evaluate differences in the magnitude of FCR and ECR muscle activity between RT and CT stabilization tasks. We then computed five estimates of average muscle co-activity values about the wrist, elbow, and shoulder joints: phase 2 (averaged across CT and RT trials), phase 3 (RT), phase 3 (CT) as well as during phases 4 and 5 (both of which were averaged across CT and RT trials). At each joint, one-way, repeated-measures ANOVA were used to test the null hypothesis that the mean muscle co-activity was equal across phases 2–5 of the stabilization trial. Dunnet's post hoc *t*-test was used to detect significant differences in co-activity during phases 2–4 from the control condition (i.e., from phase 5). Post hoc Tukey *t*-tests were also used to compare *RT* stabilization co-activity values across joints. Finally, we performed three-way, repeated-measures ANOVA and post hoc Tukey *t*-tests to compare muscle excess-activity, ExA, across trial phases (2–5), muscles, and load type at the wrist. Statistical testing was carried out within the Minitab computing environment (Minitab). Effects were considered statistically significant at the $\alpha = 0.05$ level.

RESULTS

The frequency content of both the constant and random pressure perturbations were within the bandwidth of the manipulandum (Suminski and Scheidt 2004), and thus the perturbations were consistent from one trial to the next within subjects and across the study population (see Fig. 2*A*, P_{CT} and P_{RT}). Despite this consistency, wrist angle time series were highly variable both within and across subjects. During stabilization, wrist angle deviations from the target were variably compensated within a given trial, and subjects were able to recover the desired reference position only on average across many trials (Fig. 2*B*). Not unexpectedly, subjects were less able to maintain steady hand posture while perturbed by band-limited pseudo-random torques than by constant torques. Planned, paired *t*-test found greater objective RMS wrist angle errors in RT versus CT trials in both the MRI ($T_{10} = 7.62$, $P < 0.0005$) and mock-MRI ($T_{10} = 11.94$, $P = 0.0005$) experimental sessions. Thus subjects demonstrated similar behavioral trends in both sessions. In the MRI session, RMS wrist angle errors did not differ as a function of trial number, providing no evidence of performance improvements with extended practice in either stabilization task [CT: $F(4,41) = 0.81$, $P = 0.524$; RT: $F(4,41) = 0.37$, $P = 0.823$]. We also observed significant positional drift over time in 91% of RT trials (88 of 96) and 75% of CT trials (72 of 95). The absolute magnitude of this drift was 0.155 ± 0.104°/s and 0.017 ± 0.028°/s in the RT and CT cases, respectively. In both torque conditions, the drift was evenly distributed about the target angle and appeared to vary randomly from one trial to the next. Similar trends were observed in the mock-MRI experimental session.

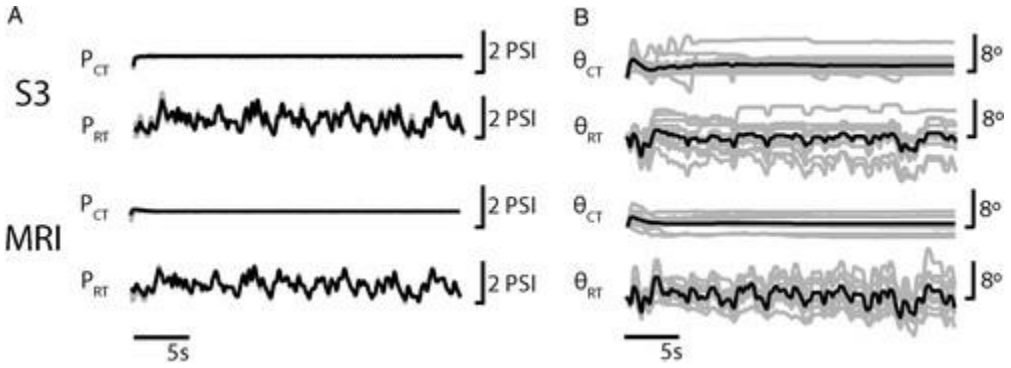

FIG. 2.*A*: measured bellows pressure for both a representative single subject (*top, S3*) and the subject population tested within the MR scanner experiment (*bottom*, MRI) while stabilizing against either constant (P_{CT}) or random (P_{RT}) torque perturbations. *B*: wrist angle error for both a representative single subject (*top, S3*) and the population of the MR scanner experiment (*bottom,* MRI). For the representative subject (*top*), light gray lines indicate the subject's performance on individual trials, whereas heavy black lines denote the mean performance of the subject across trials. For the population (*bottom*), light gray lines indicate the mean performance of individual subjects and the heavy black lines denote the mean performance of the population.

In the MRI experimental session, we observed discrete corrective movements (Fig. 3*A*) in joint angle trajectories in 95% of RT trials (91 of 96) and 19% of CT trials (18 of 95). Of these corrective movements, 51% and 62% were flexion movements in the RT and CT cases, respectively. The majority of corrective movements were directed appropriately to reduce positioning errors (56.1 and 80% of movements in the RT and CT cases, respectively; (shaded bars in Fig. 3, *B* and *C,* represent correctly directed movements). Again, similar trends were observed in the mock-MRI session.

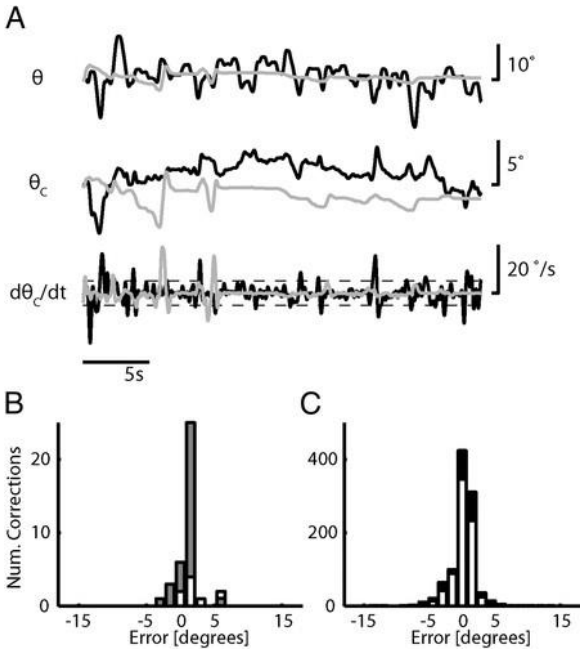

FIG. 3.*A*: raw joint angle time series (θ; *top*) for representative RT (black) and CT (gray) stabilization trials. To facilitate identification of events consistent with the resetting of behavioral goals (i.e., discrete corrective movements), for each stabilization condition for each subject, we removed the average wrist angle trajectory from every individual trial to obtain corrected wrist angle time series (θ_C; *middle*). We considered as corrections only those movements wherein the angular velocity of corrected wrist angle trajectories exceeded 5°/s, occurring ≥1 s after the start of a stabilization period ($d\theta_C/dt$; *bottom*). *B*: subjects executed discrete corrective movements in a direction to reduce the magnitude of positioning errors in 80% of CT trials where discrete

movements were observed (□) and (*C*) in 56.1% of RT trials wherein discrete movements were observed (▪). In both cases, incorrectly directed movements are superimposed (not stacked) in white.

Figure 4*A* compares kinematic performance and EMG activity during both RT and CT stabilization for a representative subject in phases 2–5 of the mock-MRI experiment. Preprogrammed (commanded) changes in wrist torque (τ_c) elicited changes in wrist angle (θ) and wrist angular velocity (dθ/d*t*) despite instruction to hold the hand steady at the target angle. Whereas the RT perturbations in phase 3 elicited joint angular deflections that persisted throughout the stabilization period, averaging 16.95 ± 3.07° peak to peak across subjects and trials, CT perturbations elicited only transient hand deflections averaging 6.07 ± 2.07° peak to peak across subjects and trials. At the wrist, increases in both flexor FCR and extensor ECR activities were consistently observed in both torque conditions. Across subjects, average FCR activity increased by 13.1 ± 5.3% of its MVIC level in the RT case relative to rest, whereas it increased by only 7.4 ± 3.5% in the CT case. Activities were greater in the RT case (T_{10} = 6.35, P < 0.0005). Average ECR activity increased by 10.6 ± 4.3% of its MVIC level in the RT case relative to rest, whereas it increased by only 2.6 ± 1.5% in the CT case. Again, activities were greater in the RT case (T_{10} = 7.18, P < 0.0005). Not surprisingly, the variability of EMG activity was also consistently much greater in the RT case for both muscles. Although not shown in Fig. 4, we similarly examined the synergistic flexors FDS and FCU and found their patterns of activation to mirror those of FCR closely. Cross-correlation analyses between the activations of FCR and each of these flexors yielded single peaks with no time lag. Similarly, the synergistic extensors EDC and ECU mirrored activations in ECR closely. Consequently, we limited further analysis of wrist musculature to FCR and ECR.

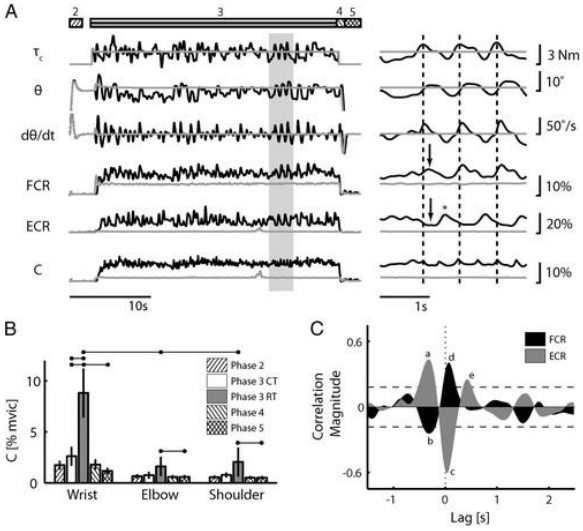

FIG. 4.EMG and kinematic data demonstrated that subjects utilize a combination of reciprocal activation and antagonist muscle co-activation to stabilize the wrist. *A*: kinematic and EMG data from a representative subject during phases 2–5 (bar at top) of RT (black traces) and CT (gray traces) trials in the mock-MRI experiment. Phase 2 consists of the time period where subjects are passively moved from a resting position (40° wrist flexion) to the stabilization target angle (20° wrist flexion) ~3 s prior to the start of stabilization. During phase 3, subjects actively stabilize their wrist for 30 s against either a CT or RT perturbation. Phase 4 consists of passive movement of the subject from the stabilization target angle back to the resting position, and during phase 5, subjects are instructed to rest quietly. Preprogrammed changes in commanded wrist torque (τ_c) elicited changes in wrist angle (θ) and wrist angular velocity (dθ/d*t*) despite instructions to hold the hand steady at the target (initial) joint angle. Note the rapid changes in θ and dθ/d*t* during phases 2 and 4 while subjects are being passively moved. EMG activity in both flexor carpi radialis (FCR) and extensor carpi radialis (ECR) was negligible during the passive movement and resting states (phases 2, 4, and 5). Activity in both FCR and ECR was significantly greater in RT trials as compared with CT trials. In the CT case, transient increases in co-activation *C* measured at the

onset of stabilization approach a steady-state value within ~500 ms. In the RT trials, co-activity *C* increased dramatically over both baseline and that estimated during CT trials. Time series of selected kinematic and EMG variables on an inflated time scale (gray bar in *A*) is shown in *A, right*. Rapid increases in commanded wrist torque τ_c elicit rapid wrist extensions (dashed vertical markers) that led increases in FCR activity and decreases in ECR activity, both with relatively short latencies (single arrowheads). Increased extensor activity consistent with a strategy of increased co-activity is evident much later (asterisk). *B*: averaged population data demonstrated that antagonist muscle co-activity *C* was greatest at the wrist during stabilization (phase 3) in both torque tasks as compared with rest (phase 5) although it was significantly greater in RT trials compared with CT trials. Co-activity was also present at the elbow and shoulder but only during RT trials. Co-activity at the wrist was greater than at the elbow and shoulder on RT trials. Horizontal bars indicate significant differences between stabilization conditions at the $P < 0.05$ level. Hatched bars, estimates of co-activity during phases 2, 4, and 5; white and gray bars, estimates of co-activity during periods of active stabilization (phase 3) against CT and RT, respectively. Error bars indicate ±2 SEs of the mean. *C*: cross-correlation analysis of $d\theta/dt$ and FCR (black area) or ECR (gray area) for a representative subject. Significant correlations were observed with EMG both lagging/leading changes in $d\theta/dt$. The horizontal dashed lines represent the 95% confidence interval about 0 correlation. Peaks of significant FCR correlations with $d\theta/dt$ were observed at −320 ms (b) and 60 ms (d), and the peaks of *ECR* correlations with $d\theta/dt$ were observed at −310 ms (a), 23 ms (c), and 405 ms (e).

At the wrist, ANOVA and post hoc Dunnet's *t*-tests found a significant effect of trial phase on muscle co-activity values [$F(4,66) = 61.33$, $P < 0.0005$; Fig. 4*B*] with elevated co-activation during phase 3 in both torque conditions relative to rest (phase 5; RT: $P < 0.0005$; CT: $P = 0.031$). Post hoc *t*-tests also showed that antagonist phase 3 co-activation at the wrist was greater on RT trials as compared with CT trials ($P < 0.05$). Elevations in co-activity were also observed at the elbow [$F(4,66) = 11.83$, $P < 0.0005$] and at the shoulder [$F(4,66) = 8.27$, $P = 0.0005$] but only during phase 3 of the RT condition ($P < 0.0005$ for both elbow and shoulder). Post hoc *t*-tests also found that co-activation in the RT condition was greater at the wrist than either the elbow ($T_{10} = 6.21$, $P < 0.0005$) or the shoulder ($T_{10} = 5.71$, $P < 0.0005$). There was no difference in magnitude of co-activation in the RT condition between the elbow and shoulder ($T_{10} = 0.49$, $P = 0.633$). No significant EMG activity was observed during passive movement (phases 2 and 4) as compared with rest at any joint.

Examination of the ExA's revealed that during stabilization, the magnitude of muscle activations potentially contributing to long-loop feedback compensation for positioning errors varied by trial phase [$F(3,138) = 14.64$; $P < 0.0005$] and muscle [$F(1,138) = 22.32$; $P < 0.0005$] and not by trial type [$F(1,138) = 0.36$; $P = 0.552$]. Post hoc Dunnet's *t*-test found elevated excess EMG activations during active stabilization relative to rest (phase 3: $P < 0.0005$) but not during periods where the wrist was passively moved (phase 2: $P = 0.084$; phase 4: $P = 0.757$). Additional post hoc Tukey's *t*-tests reveled that the magnitude of this phasic muscle activation was greater in the FCR that in the ECR ($P < 0.0005$), a finding consistent with the expected activation patterns given the biased perturbations used in this study.

We next performed a correlation analysis between changes in wrist angle and measured EMG responses in the RT condition to evaluate the contributions of reflex-mediated responses to wrist stabilization (Fig. 4C). For the wrist flexor FCR, we consistently observed increased EMG activity lagging wrist extension (i.e., increases in $d\theta/dt$ by the convention used in Fig. 4) by 59.0 ± 44.2 ms (range: 20–178 ms; Fig. 4*C*, d). The timing of this load-dependent activity was within the range of delays expected for long-loop reflex compensation for muscle stretch (Evarts and Vaughn 1978; Matthews 1981; Strick 1978). For the wrist extensor *ECR*, we consistently observed decreased EMG activity lagging wrist extension by 40.3 ± 23.7 ms (range: 17–93 ms; Fig. 4*C*, c). The sign and latency of these EMG changes are consistent with an unloading response (Sinkjaer et al. 2000). We also observed an increase in *ECR* activity with lag of 484.8 ± 118.3 ms (range: 387–675 ms; Fig. 4*C*, e) in 5/10 subjects. This later response is consistent with a strategy of voluntary co-activation about the wrist because no

contemporaneous decrease in flexor activity is observed. Finally, for both muscles, we observed that EMG led $d\theta/dt$ by ~350 ms (Fig. 4*C*, a and b); this correlation between changes in EMG activity and later changes in $d\theta/dt$ are obligated by the compliance of the pneumatic device. These relationships are evident on closer examination of individual EMG responses (Fig. 4*A*, *right*, inflated time scale).

Functional imaging

We sought to identify the neural correlates of wrist stabilization mediated by long-loop reflex (feedback) control and muscle co-activation strategies during experiments conducted within the MR scanner. Changes in BOLD signal intensity relative to rest were correlated with either periods of deterministic CT or unpredictable RT wrist stabilization in many cortical and subcortical regions thought to contribute to movement and stabilization of the upper extremity (Table 1, $p_{corrected} < 0.05$; Fig. 5*A*). We examined the time series of BOLD activations for each ROI identified in Table 1 during stabilization against each load type for each subject. Two basic patterns of activation became evident. The first, an example of which is shown in Fig. 5*B* for the ROI spanning the primary sensorimotor cortex (M1/S1), was characterized by sustained increases in percentage BOLD signal change (PSC) during RT stabilization and only transient increases in PSC during passive movement of the hand (i.e., starting before the onset of CT stabilization). The second pattern, an example of which is shown for the right middle frontal gyrus (BA 46), was characterized by a parallel increase in PSC during both stabilization conditions with no sensitivity to passive movement. A third example, shown for the cerebellum ROI, shows some sensitivity to stabilization type, but little sensitivity to passive movement. Using features which quantify these subjective observations, we performed a k-means cluster analysis to identify those ROIs demonstrating common patterns of sensitivity to trial type and/or passive movement (see methods). Two distinct groups were identified: those ROIs that were sensitive to both trial type and passive movement (cluster 1; red regions in Fig. 5*A*), and those demonstrating increased BOLD activation over the duration of the trial, and largely insensitive to passive movement (cluster 2; blue regions in Fig. 5*A*). Group separation and membership was visualized by plotting the coordinates of each ROI within the Ψ plane (Fig. 5*C*) where cluster 1 membership is indicated by red circles, and cluster 2 membership is indicated by blue squares (see also Table 1). Cluster 1 contained ROIs located in left precentral, postcentral, middle frontal gyri, including primary motor cortex (M1, BA 4), primary sensory cortex (S1, BA 2 and 3), and the dorsal premotor cortex (PMd). Additional cortical ROIs with membership in cluster 1 included the left superior/inferior parietal lobule (SPL/IPL, BA 5 and 7), right precentral gyrus (PMd and PMv, BA 6), middle temporal gyrus (MTG, BA 39), bilateral medial frontal gyrus (SMA, BA 6), and the caudal cingulate gyrus (CCZ) (Picard and Strick 2001). There were no subcortical ROIs contained in cluster 1. Cluster 2 contained ROIs located in right PMd, bilateral SMA, and the cingulate gyrus (although these ROIs were located rostral to the vertical anterior commissure line and are thus considered to be located in pre-PMd), pre-SMA, and the rostral cingulate zone (RCZ) (Picard and Strick 2001). In addition, Cluster II contained cortical ROIs located in the left superior frontal gyrus (SFG, BA 8), medial frontal gyrus (MeFG, BA 8), angular gyrus, bilateral IPL (BA 40), middle frontal gyrus (MiFG, BA 10 and 46), inferior frontal gyrus (IFG, BA 45, 46 and 47), supramarginal gyrus, superior temporal gyrus (STG, BA 22) and insula (BA 13). Cluster II contained subcortical ROIs in the basal ganglia, cerebellum, and thalamus. The ROI in the left basal ganglia included activation of the putamen, globus pallidus, and caudate body, whereas the cerebellar ROI was localized in the bilateral cerebellar cortex lobules IV, V, and VI (Schmahmann 2000), vermis, and the right dentate nucleus (DN). ROIs in the thalamus exhibited activations in the left ventral posterior lateral (VPL) nucleus, ventral lateral (VL), ventral posterior medial (VPM), ventral anterior (VA), medial dorsal (MD) nuclei, and left pulvinar. Regions showing significant sensitivity to passive movement, i.e., $\bar{S} \neq 0$, [$F(18,162) = 2.37$; $p_{corrected} < 0.05$] are indicated by filled symbols. These include left M1/S1, SPL/IPL (BA 5 and 7), and SMA/CCZ. The left M1/S1, SPL/IPL (BA 5 and 7), and right STG (BA 39) were also significantly modulated by task type, with $\Delta_M > 0$ [$F(18,162) = 3.94$; $P < 0.05$].

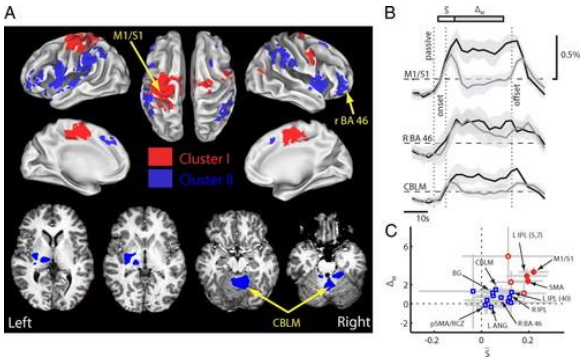

FIG. 5.*A*: functional activation maps for the study population showing the regions of interest (ROIs) activated during periods of either random (RT) or constant (CT) torque stabilization. Colored areas indicate regions that were shown to be significantly active in these contrasts at the $P < 0.05$ level of significance (corrected for multiple comparisons). ROIs categorized into cluster I by the k-means cluster analysis are shown in red and ROIs placed into Cluster II are shown in blue. *Top*: activations mapped onto inflated representations of the cerebral hemispheres; *bottom*: subcortical activations in the basal ganglia and thalamus (left: $z = 6$; center-left: $z = 1$), anterior cerebellar cortex (center right: $z = -12$), and right dentate nucleus (right: $z = -20$). *B*: Percent signal change (PSC) and cluster analysis of blood-oxygen-level-dependent (BOLD) time series from RT (black lines) and CT (gray lines) stabilization periods. The shaded regions about each time series indicate ±2 SE. The scale bars above the PSC plots indicate the time intervals used to calculate the components of $\Psi = \{\bar{S}, \Delta_M\}$. The $\bar{S}$ feature was the average of 4 consecutive data points from each of the RT and CT trials, beginning 2 points prior to the start of the stabilization period. The Δ_M feature was computed as the difference between the average RT and CT PSC time series during the middle 20 s (8 TR) of stabilization. Two distinct patterns were observed. ROI time series taken from M1/S1/PMd are representative of the first pattern of activation (cluster 1). Activations in cluster 1 are sensitive to perturbation type in that RT trials show increased activity over the duration of the 30-s stabilization period, whereas CT trials have increased activation only at the beginning and end of the trials when the hand is moved passively and the perturbation changes on-off state. Activities taken from the right middle frontal gyrus (BA 46) are representative of the second pattern of activation (cluster 2). Cluster 2 ROIs show parallel increases in BOLD PSC with little differentiation between RT and CT stabilization trials. Many of these regions are also insensitive to passive movement. The ROI time series taken from the cerebellum (CBLM) is representative of ROIs near the boundary between cluster groups 1 and 2. These ROIs show some sensitivity to stabilization type, but little sensitivity to passive movement. *C*: group separation and membership for the 18 ROIs considered in the k-means cluster analysis was visualized by plotting the coordinates of each ROI within the Ψ –plane. Cluster 1 membership is indicated by the red circles and cluster 2 membership is indicated by the blue squares (see also Table 1 for a description of ROI location). Regions showing significant sensitivity to passive movement, i.e., $\bar{S} \neq 0$, are indicated by filled symbols. These include left M1/S1/PMd, IPL (BA 5 and 7), and SMA/CCZ. M1/S1, primary sensorimotor cortex; L IPL (5,7), left inferior parietal lobule (BA 5,7); L IPL (40), left inferior parietal lobule/supramarginal gyrus; L ANG, left angular gyrus/inferior parietal lobule; SMA, supplementary motor area; CBLM, bilateral cerebellar cortex and right dentate nucleus; BG, basal ganglia and thalamus; R BA 46, right middle/inferior frontal gyrus; pSMA/RCZ, presupplementary motor area and rostral cingulate zone; R IPL (40), right inferior parietal lobule/supramarginal gyrus.

We next evaluated whether the activations identified in the preceding analysis were related to compensation for kinematic errors, generation of wrist torques, or both. We constructed contrasts wherein one-sided *t*-test (corrected for multiple comparisons) evaluated whether BOLD activation changes were correlated with RMS state estimation errors or RMS torques either on a trial-by-trial or a TR-by-TR basis ($\text{Error}_{\text{Trial}}$, Error_{TR}, $\text{Torque}_{\text{Trial}}$, and $\text{Torque}_{\text{TR}}$; Fig. 6). The $\text{Error}_{\text{Trial}}$ contrast (Fig. 6; blue regions; $p_{\text{corrected}} < 0.05$) reveals areas of activation in the left IPL (BA 40, *A* and *B*), angular gyrus (*A* and *B*), RCZ (BA 32, *A*), and right MiFG (BA 46, *C*). Alternatively, the Error_{TR} contrast (Fig. 6; red regions; $p_{\text{corrected}} < 0.05$) reveals areas of elevated BOLD activation in the left

precentral (M1, BA 4), postcentral (BA 3 and 5), middle frontal (PM_d, BA 6), right precentral gyri (PM_v, BA 6), bilateral SMA proper and CCZ similar to regions with membership in cluster 1 (*A*–*C*). Additional cortical activations were observed in right MeFG (BA 8, *C*), supramarginal gyrus, IFG (BA 46, *C*), STG (BA 22, *C*), bilateral IPL (BA 40, *B* and *C*), and insula (BA 13, *C*). Subcortical activations were observed in the left putamen, globus pallidus (medial and lateral), VL, VPL, VPM nuclei of the thalamus (*D*), the right cerebellar cortex (lobule IV, V, and VI; *E* and *F*) and the red nucleus. Activation of the left IPL in the $Error_{Trial}$ contrast were located more posterior to those activated regions of IPL in the $Error_{TR}$ contrast. There were no overlapping activations in the $Error_{Trial}$ and $Error_{TR}$ contrasts. Importantly, no regions were found to be active in contrasts examining differences between $Torque_{Trial}$ or $Torque_{TR}$ and resting baseline.

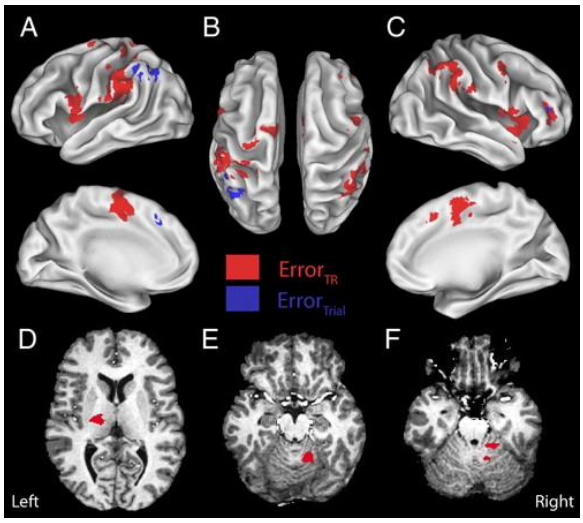

FIG. 6. Functional activation maps for the study population showing those regions wherein the BOLD response correlated significantly ($P < 0.05$, corrected for multiple comparisons) with state estimation errors on both a moment-by-moment ($Error_{TR}$, red regions) and a trial-by-trial basis ($Error_{Trial}$, blue regions). Activations in the $Error_{TR}$ contrast are localized primarily within regions identified to have membership in cluster 1 including the left precentral (M1, BA 4), postcentral (BA 3 and 5), middle frontal (PMd, BA 6), right precentral gyri (PMv, BA 6), bilateral SMA proper and CCZ (*A*–*C*). Other cortical and subcortical activations correlating with moment-by-moment changes in error were observed in cluster 2 regions including the right MeFG, supramarginal gyrus, IFG, STG, cerebellar cortex (*E; z* = −13) bilateral IPL, insula, and left VL, VPL, VPM nuclei of the thalamus (*D*; *z* = 9). Alternatively, the $Error_{Trial}$ contrast reveals only cluster 2 cortical activation in the left IPL, angular gyrus, RCZ (BA 32, and right MiFG in *A*–*C*). No BOLD correlations with wrist torque were observed on either a trial-by-trial or a moment-by-moment basis.

Although not shown, we similarly evaluated whether BOLD activations were correlated with moment-by-moment fluctuations in objective stabilization errors on a TR-by-TR basis [i.e., by replacing ε_s(nT) with ε_o(nT) in *Eq. 7*]. We found activation regions similar to those displayed in red in Fig. 6, although activation within M1 did not reach statistical significance using the thresholding and clustering criteria reported above. In contrast, when we evaluated whether BOLD activations were correlated with subjective stabilization errors on a trial-by-trial basis $RMS_{TRIAL}(\varepsilon_s)$, we found no regions with significant activation. Thus distinct neural networks appear to be involved in the processing of separate estimates of kinematic performance errors over short and long time frames.

Next, we performed a BOLD contrast highlighting brain regions that were differentially active in the random and constant torque stabilization tasks. Based on the behavioral and EMG results obtained in the mock-MRI study, this contrast is expected to identify brain regions acting to elevate peripheral joint co-activity as well as regions involved in the feedback stabilization of the wrist, exclusive of regions contributing similarly to the

compensation for average extensor torques which were common to both tasks. A mixed-model ANOVA treating subjects as the random factor contrasted the BOLD responses to stabilization against random and constant torque perturbations (RT > CT, Fig. 7, purple ROIs; $p_{corrected}$ <0.05). This contrast reveals areas of elevated activation in left primary sensorimotor cortex extending into PMd proper, rostral portions of IPL (BA 40) and SPL (BA 5), and bilateral SMA proper and CCZ (*A*–*C*). Additional cortical activations are also observed in the left STG (BA 41, *A*), right primary sensorimotor cortex (*B* and *C*), PMd, and the bilateral insula (*A* and *C*). Subcortical activations were observed in the left MD, bilateral VL, VPL, and VA nuclei of the thalamus (*D*) and bilateral basal ganglia (caudate/putamen/globus pallidus; left hemisphere activation shown in *D*), and the left red nucleus. Bilateral activations are observed in anterior cerebellar cortex (*E* and *F*), while activation is also evident in the right dentate nucleus (*F*). In contrast, no regions of elevated activity were found in a mixed-model ANOVA contrasting CT > RT.

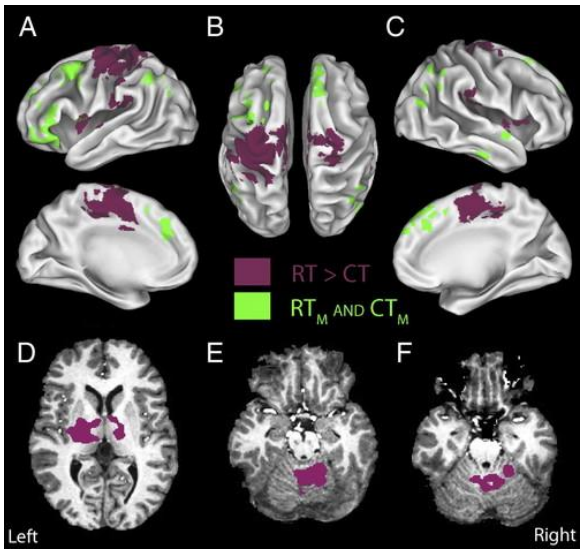

FIG. 7. Functional activation maps for the study population showing the RT > CT (purple regions) and the RT_M and CT_M contrasts (green regions). Colored areas indicate regions that were shown to be significantly active in these contrasts at the $P < 0.05$ level of significance (corrected for multiple comparisons). The RT > CT contrast reveals activations largely lateralized in left primary sensorimotor cortex (extending into PMd proper), SMA proper, and rostral portions of IPL in *A* and *B.* Activations observed in the RT_M AND CT_M contrast were observed in left pre-PMd, inferior frontal gyrus, bilateral pre-SMA, superior/middle temporal gyrus, and the right superior frontal gyrus as shown in *A*–*C* and are representative of the generation of discrete corrective movements. Activations in the RT > CT contrast also include subcortical regions: left thalamus and basal ganglia (*D; z* = 7), bilateral anterior cerebellar cortex lobule IV, V, and VI (*E* and *F, z* = −10), and the right dentate nucleus (*F, z* = −20).

Finally, we performed an analysis highlighting brain regions that were commonly active throughout the stabilization period in both torque conditions, disregarding activations that may have arisen due to passive movement of the hand and/or other transient events at the beginning and end of trial phase 3. Therefore we limited this final BOLD analysis to the middle third of the stabilization time series. We constructed a contrast including all voxels wherein *t*-test (corrected for multiple comparisons) found BOLD activations to exceed their resting values. We then identified those regions having similar activations in both stabilization conditions (i.e., the intersection of the group activation maps for RT_M and CT_M; Fig. 7, RT_M and CT_M; green ROIs, $p_{corrected}$ <0.05). This contrast reveals areas of elevated activation in left pre-PMd, IFG (BA 10, 45, 46, and 47; *A*), STG (BA 22, *A*), bilateral IPL, STG, MTG (*A* and *C*) pre-SMA (*A*–*C*), and right superior frontal gyrus (BA 8, *B*).

DISCUSSION

Subjects performed two sets of identical experiments, both in and out of a MR scanner, wherein they stabilized their wrists against predictable and unpredictable torque perturbations. Kinematic and EMG data revealed that subjects compensated for the different perturbations using a flexible combination of three simple strategies. These included: the modulation of joint viscoelasticity via co-activation of agonist/antagonist muscle pairs spanning the wrist, elbow, and shoulder joints, spinal and supraspinal reflex action, and the generation of discrete corrective movements. Whereas cocontraction and spinal reflex action are considered to be peripheral response mechanisms that can be influenced by descending motor commands (Porter and Lemon 1995), supraspinal (long-loop) reflex action and the generation of discrete corrective movements both depend on transcortical neural processing (Evarts and Tanji 1976; Haaland and Harrington 1989; Strick 1983). We sought to test the hypothesis that during stabilization of the wrist, distinct neural mechanisms contribute to the closed-loop feedback control of wrist position and the evaluation/adjustment of controller parameters (e.g., the desired reference wrist angle) in response to persistent performance errors. We expected that BOLD signal activity in regions mediating on-line feedback control of endpoint position would be sensitive to moment-by-moment variations in state estimation errors, not torque, consistent with their putative role in the optimal feedback control of movement (Scott 2004). We expected BOLD signal activity in brain regions that monitor and adjust the performance of the feedback controller to be sensitive to variations in performance errors over a much broader time frame. This prediction derives from the control theoretic consideration that stability of nested control loops (such as those proposed here) requires that supervisory updating of behavioral goals and/or feedback control laws must have lower bandwidth (i.e., process information at a slower rate) than the closed-loop feedback controller being monitored and adjusted (cf. Widrow and Walach 1996). Consistent with our hypothesis, the experimental results provide EMG, kinematic, and functional imaging evidence in support of the ideas that separate neural mechanisms control posture and discrete corrective motions of the wrist during stabilization and that kinematic performance errors are processed over very different time scales in the networks serving these functions.

Flexible combination of control actions in the stabilization of wrist position

The conclusions that subjects invoked multiple control actions to stabilize the hand and that the particular combination of strategies varied by load type were drawn from the EMG and kinematic observations presented in Figs. 3 and 4. Both segmental and long-loop reflex actions likely contributed to stabilization because we observed temporal correlation between wrist flexor FCR EMGs and the rate of change in wrist joint angle during RT stabilization at latencies between 20 and 178 ms. Loop delays on the short end of this range are consistent with the presence of M1 responses arising from monosynaptic reflex pathways (Lee and Tatton 1975). Loop delays on the long end of the range are consistent with long-loop responses mediated by transcortical pathways thought to transit primary sensorimotor cortex (Evarts and Tanji 1976; Thach 1978) and the cerebellum (Strick 1978, 1983; Thach 1978). The presence of long-loop reflex action provides a means by which the brain can implement closed-loop feedback control over wrist position (Evarts and Fromm 1981; Evarts and Tanji 1976; Miall et al. 1993; Strick 1978). The same correlation analysis revealed that a strategy of co-activation of wrist antagonist muscles was evident much later, at a lag of ~500 ms in 5 of 10 subjects (range: 387–675 ms; Fig. 4*C*, e).

Analysis of muscle activity time series revealed that agonist/antagonist co-activity increased dramatically more during RT than CT stabilization (yet was absent during passive movement of the wrist; Fig. 4*B*). Increasing the level of antagonist muscle co-activity is an effective compensatory strategy because it increases joint viscoelasticity about the specified limb equilibrium configuration (Gomi and Osu 1998; Lacquaniti et al. 1993). However, the ubiquitous presence of drift in stabilized wrist positions demonstrates that the desired equilibrium angle (i.e., the reference wrist angle for on-line feedback control) is subject to the spontaneous accumulation of

position errors. Importantly, discrete corrective actions were evident in the wrist angle time series in both stabilization tasks evidently in response to this drift. The directions of these corrections were objectively accurate in 80% of the CT stabilization cases, suggesting that a separate, more accurate representation of desired position was likely used both for evaluating the efficacy of the moment-by-moment control and for the planning and execution of discrete corrective adjustments to the reference wrist angle. If a common representation of reference wrist configuration was used for both on-line feedback and for the planning of corrective adjustments, there would have been no mismatch between the realized hand position and the reference angle used by the processes monitoring the performance of the on-line feedback controller. Consequently, there should have been few corrective movements observed during CT stabilization when in fact we observed corrections in nearly 20% of the trials. We therefore conclude that the brain maintains separate representations of target location for the regulation of limb posture and the planning of discrete corrective movements.

Invoking multiple control strategies during limb stabilization is a rational policy to employ because the strengths of each strategy offset weaknesses in the others. Impedance control, the regulation of joint viscoelasticity about a desired limb configuration, was implicated by significant increases in co-contraction at the wrist during both RT and CT stabilization. Impedance control is effective in reducing consequences of unpredictable perturbations (Gomi and Osu 1998; Hogan 1985; Lacquaniti et al. 1993; Milner 2002; Mussa-Ivaldi et al. 1985) because the inherent mechanical properties of muscles provide a near instantaneous response to perturbation (Loeb et al. 1999; Nichols and Houk 1976). However, impedance control incurs high energetic costs when the environmental load is biased (as it was here). These costs can be minimized using closed-loop feedback control to reduce deviations from the desired reference posture. In feedback control, sensory estimates of performance errors are transformed into motor commands which act to oppose or reduce the errors by activating only those muscles directly opposing the current load (thus eliminating “wasted” cocontractions). Unfortunately, substantial feedback delays inherent in sensory transduction, action potential propagation and transcortical feedback processing limit the overall feedback gains that can be applied practicably without inducing positional instabilities (Rack 1981), thereby limiting the effectiveness of feedback strategies in reducing bias errors. Fortunately, it is a simple matter to cancel biases through discrete adjustments to the reference or equilibrium positions of the feedback and/or impedance controllers, a behavior which we evidently observed during both RT and CT stabilization (e.g., Fig. 3, *B* and *C*). However, to ensure overall stability of performance, the mechanisms monitoring and correcting for bias in this way need to differentiate between persistent errors (which require adjustment of the reference configuration) and transient errors (which the feedback controller will soon correct). That is, whereas impedance and feedback position controllers must process kinematic performance errors on a moment-by-moment basis, mechanisms that monitor feedback performance and update performance goals should process errors on a longer time scale. If instead, error processing proceeded on the same time scale, performance errors would give rise to both feedback corrections and adjustments of the reference configuration, thus leading to an unending cycle of increasing overcompensation.

Neural correlates of wrist stabilization…

Neuroimaging contrasts revealed significant increases in BOLD activation not only in brain regions thought to contribute to the feedback control of wrist position but also in areas implicated in the ongoing evaluation of task performance and the feed-forward planning/execution of internally generated discrete movements. We evaluated the temporal evolution of BOLD activation within these regions, identifying at least two distinct cortical/subcortical networks that were differentially excited in the two stabilization tasks. The first (cluster 1) included a cerebello-thalamo-cortical network thought to contribute to the on-line computation and feedback correction of errors (Evarts and Vaughn 1978; Horne and Butler 1995; Lee and Tatton 1975; Marsden et al. 1972, 1978; Strick 1978). Consistent with this hypothesis, BOLD signal changes within these regions were

correlated with the moment-by-moment modulation of state estimation errors (Fig. 6, red regions; 2.5-s RMS integration period). That is, BOLD activity in these regions was elevated mainly during random torque perturbations and during passive movement of the hand despite the absence of significant muscle activation during passive manipulation in the behavioral experiments and the production of the same average wrist torques in both tasks. A second network (cluster 2) exhibited commonly elevated BOLD activity during performance of both stabilization tasks. Brain regions demonstrating this pattern include the prefrontal cortex, rostral aspects of dorsal premotor and SMA cortices, and inferior aspects of posterior parietal cortex. These brain regions have previously been reported to contribute to the planning and execution of internally-generated, discrete motor actions (Jahanshahi et al. 1995; Jueptner and Weiller 1998; Sakai et al. 1999; Winstein et al. 1997) and may have been involved here in resetting the reference wrist angle when on-line (moment-by-moment) feedback control failed to satisfy subjective performance constraints. Consistent with this interpretation, a subset of Cluster II ROIs were highly sensitive to state estimation errors over a much longer timeframe (Fig. 6, blue regions; 30-s RMS integration period).

…via closed-loop feedback control

Cluster 1 membership resembles the activation map produced by the RT > CT contrast (Fig. 7, purple regions) due to the differences in activation level of these ROIs during the middle phase of the two stabilization tasks (i.e., Δ_M). The RT > CT contrast shows increased activation during RT stabilization in a cerebello-thalamo-cortical network including primary sensorimotor cortex, PMd, SMA, IPL, VL thalamus, anterior cerebellar cortex, and the dentate nucleus. Because the trial types differed in antagonist co-activity levels, it might reasonably be suggested that the task dependent increase in BOLD activation during RT trials derives from differences in muscle activation and/or force output between RT and CT stabilization (Dai et al. 2001; Thickbroom et al. 1998). This does not appear to be an adequate explanation for our results for at least three reasons: first, cluster 1 regions were strongly activated during phase 2 of both stabilization trials wherein the hand was passively moved by the robot to the target position and no coincident activation in either the flexor or extensor muscles was observed (Figs. 4*A* and 5). Second, significant BOLD activation was not observed throughout the CT stabilization trials in this network despite the fact that CT trials required the same average torque production as RT trials (cf. the time series from M1/S1 in Fig. 5B and the RT_M and CT_M contrast of Fig. 7). Third, BOLD activations in many of these regions were strongly correlated with the moment by moment (TR-by-TR) variations in state estimation errors and *not variations in wrist torque output* (Fig. 6; red regions). We therefore conclude that the task-dependent increase in cluster 1 BOLD activation reflects the estimation of (and on-line feedback correction for) kinematic performance errors.

The hypothesis that the cerebellum and its input/output pathways (including posterior parietal cortex) contribute to the detection and correction of movement errors is consistent both with findings of single-unit recording studies of reaching movements in nonhuman primates (Horne and Butler 1995; Kitazawa et al. 1998; Norris et al. 2004) and human psychophysical studies of pointing to visual targets involving either neuroimaging (Desmurget et al. 2001) or transcranial magnetic stimulation (TMS) (Desmurget et al. 1999). In monkeys trained to produce rapid pointing movements to visually presented targets, Purkinje cells in the intermediate and lateral cerebellar hemispheres (lobules IV–VI) encode positioning errors (i.e., the hand position relative to the target) at the end of movement [although they appear to encode the intended final hand position at the beginning of a reach, (Kitazawa et al. 1998)]. In human psychophysical studies by Desmurget and colleagues (1999, 2001), subjects smoothly and accurately corrected reach trajectories when displacements in the visual target location were introduced after subjects initiated an ocular saccade toward the target, (i.e., during the saccadic suppression period). These findings clearly demonstrate on-line feedback correction for targeting errors during the evolving reach. Hand-path corrections were disrupted by transcranial magnetic stimulation (TMS) of the posterior parietal cortex during target presentation, although movements without

target jumps were unaffected (Desmurget et al. 1999). Using positron emission tomography (PET) Desmurget and colleagues (2001) found that these feedback corrections were mediated by a restricted network involving the posterior parietal cortex, anterior cerebellum, and primary motor cortex (Desmurget et al. 2001), whereas in a separate case study, a patient with bilateral lesions to the posterior parietal cortex was unable to make these fast "automatic" corrections for target jumps (Pisella et al. 2000). TMS has also been used to implicate parietal cortex along the anterior-lateral bank of the intraparietal sulcus (aIPS) in the "on-line control of reach-to-grasp movements" (Tunik et al. 2005). In a fMRI study requiring subjects to maneuver a joystick-controlled cursor between visual targets of various sizes (Seidler et al. 2004), BOLD activations in the CCZ, PMv, and multiple cerebellar regions were found to co-vary with target size and thus with varying demands on feedback control. And in a recent fMRI study of reach adaptation to mechanical and visuomotor perturbations, Diedrichsen and colleagues (2005) found that regions we identified as being sensitive to moment-by-moment variations in state estimation errors (Fig. 6; red regions) were also implicated in the trial-by-trial adaptation of reaching movements (Diedrichsen et al. 2005). On the basis of our findings and the literature highlighted here, we propose that the error information processing necessary for feedback stabilization of the hand is mediated by a distributed network including the cerebellum and its input/output pathways (including portions of posterior parietal cortex) and that this type of error processing is similar to that which is needed to identify and compensate for state prediction errors resulting from inaccuracies in the forward models used during movement planning (Della-Maggiore et al. 2004; cf. Kawato and Gomi 1992).

…via internally generated corrective actions

Cluster 2 ROIs exhibited generally elevated BOLD activation during stabilization but were relatively insensitive both to trial type and to passive movement. This insensitivity is expected from regions not involved in the moment-by-moment cancellation of position errors but rather in supervisory aspects of control such as evaluating the success of an ongoing task as well as the resetting of behavioral goals when ongoing performance is deficient. Accordingly, we found that activation in a subset of cluster 2 regions correlated with changes in state estimation errors with a relatively long integration period of 30 s (Fig. 6, blue regions). In a recent study requiring subjects to maintain pinch grip force at a remembered target level or at a level indicated on a video screen, Valliancourt and colleagues suggest that activities in the dorsolateral prefrontal, ventral prefrontal, and anterior cingulate cortices are related to the retrieval and play-back of motor output from memory during internally guided actions (Vaillancourt et al. 2003). Prefrontal areas have been shown to play a role in working memory (Goldman-Rakic 1987) and task selection (Rubia et al. 2001). The anterior cingulate cortex has also been implicated in the on-line monitoring of performance in conditions wherein errors are likely to occur (Carter et al. 1998), consistent with its elevated activity in both constant and random loads in the current study because both would lead to substantial performance errors if left uncompensated. Finally, in a study of self-initiated movements (Jahanshahi et al. 1995), PET found increased activation in brain areas including many of those having cluster 2 membership in the current study. In that study, both healthy individuals and subjects with Parkinson's disease were required to perform either self-initiated or externally cued finger extension movements at a constant rate. The population with Parkinson's disease demonstrated reduced activation in a cortico-basal ganglia loop including the SMA, thalamus, and putamen; a network linked to the generation of well-timed (Rao et al. 1997) and appropriately scaled discrete movements (Desmurget et al. 2004).

In the present study, subjects generated appropriately directed corrective movements in the majority of CT stabilization trials. To generate these movements, subjects first needed to determine when error had grown sufficiently large to warrant correction (i.e., resetting the reference wrist angle) and then plan the magnitude and direction of the corrective action. Thus it is not surprising that an activation map derived from the RT_M and CT_M contrast (Fig. 6, green regions) highlights a subset of cluster 2 ROIs thought to be involved in the planning and conditional execution of movement (Deiber et al. 1997; Grafton et al. 1998; Rubia et al. 2001; Shen and

Alexander 1997). Because the cluster 2 regions implicated in error processing with a relatively long integration period of 30 s (Fig. 6, blue regions) are distinct from those involved in error processing on a moment-by-moment basis (Fig. 6, red regions), we conclude that the brain recruits distinct neural systems for closed-loop feedback control of limb position and for the evaluation/adjustment of feedback control parameters (e.g., the reference wrist angle) in response to persistent errors.

Optimality of wrist posture control

A striking feature of many cluster 1 ROIs was their responsiveness to both active and passive movements (see also Carel et al. 2000; Jueptner et al. 1997; Mima et al. 1999; Weiller et al. 1996). These included left M1/PMd, S1, IPL (BA 5 and 7), and SMA/CCZ. Similarly elevated activities were also observed in single-unit recording studies in monkeys during both active and passive movements in M1 (Fetz et al. 1980; Scott and Kalaska 1997; Wong et al. 1978), PMd (Scott et al. 1997), S1 (Soso and Fetz 1980), area 5 (Soso and Fetz 1980), and SMA (Brinkman and Porter 1979; Tanji and Kurata 1979). Passive response to imposed movement has been regarded as a hallmark of those brain regions participating in the optimal feedback control of motor activity (Scott 2004). Specifically, passive limb movement results in a mismatch error between the estimated limb state and the limb state expected given the most recent history of motor commands (efference copy) (see Wolpert and Flanagan 2001 for a review). Areas that receive or operate on this error signal would be expected to respond in a manner similar to M1/S1 and other ROIs having cluster 1 membership, and indeed BOLD responses within these regions (including the cerebellum and its output pathways) correlate with the magnitude of state estimation errors on a moment-by-moment basis (Fig. 6, red). Optimization of on-line control could be realized if a secondary, supervisory mechanism monitors the long-term performance of the feedback controller and adjusts controller parameters (including the reference wrist angle) when performance deviates from some desired value. Exactly this kind of error processing was observed here in a subset of cluster 2 ROIs (Fig. 6, blue), supporting the idea that distributed and distinct neuronal networks contribute to the optimal control of motor actions by processing performance errors over shorter and longer time scales.

Recently, Smeets and colleagues have proposed that the brain persists in maintaining an optimal estimate of limb state even when sensory feedback of limb or hand position is prevented (Smeets et al. 2005). This limb state estimate may be updated with either afferent (e.g., visual or proprioceptive) and/or efferent information about the hand's intended movements. In the absence of ongoing sensory feedback, each additional movement adds uncertainty to this estimate. Because of the amplitude-dependent variability of motor output, the estimated limb state is expected to drift with each additional movement. As would be predicted by this model, we observed significant drift throughout the majority of stabilization trials against both constant and random torque perturbations with drift magnitude and frequency being greatest during random torque stabilization wherein muscle activities are greatest and movement corrections are more frequent. This observation also provides support for the hypothesis that the brain uses an optimal estimate of limb state in the feedback control of motor activity (Scott 2004; Smeets et al. 2005). Posterior parietal cortex, which receives convergent information from visual and proprioceptive sources, is thought to compute an estimate of the current limb state for use in planning reaching movements (Buneo et al. 2002; Desmurget et al. 2001; Wolpert et al. 1998). The observation here that nonoverlapping regions of posterior parietal cortex process kinematic error information over different time scales suggests that the PPC composes multiple limb state estimates not only for the planning and execution of motor actions but also for adjusting control parameters based on the outcome of those actions.

There are at least three ways in which supervisory control functions can modify the moment-by-moment response of inner control loops. The first is by adjusting the control loop set point or reference input (i.e., by adjusting the behavioral goal) to bring the average performance of the feedback controller more in line with the representation of desired state maintained within the supervisory loop. A second is by adjusting the gains of the

feedback controller itself. This might be expected, for example, if the task objective (context) changes significantly, requiring a change in the regulated variable (e.g., from position to force or muscle activity, etc.). The third is by updating the internal model that transforms a copy of motor outflow into the estimate of desired limb state needed for computing performance errors. Updating of internal models is necessary because changes in environmental load can degrade the accuracy of their predictions (Lackner and Dizio 1994; Shadmehr and Mussa-Ivaldi 1994). While our data provide no compelling reason to preclude the later two possibilities during wrist stabilization, adjustment of the feedback setpoint was clearly observed in these experiments because the vast majority of discrete corrective movements in the CT trials were appropriately directed to reduce objective performance errors and the neural correlates of long-term error processing (Fig. 6, blue) were correlated with objective performance errors, and not state estimation errors as calculated in *Eq. 7*. Future studies should address the context-dependency of feedback control by contrasting the processing of performance errors in tasks requiring accuracy either in the control of endpoint force, muscle activity level or endpoint position when the limb is excited by controlled perturbations. If the brain does indeed instantiate optimal feedback control of motor function, results similar to those presented here in Figs. 6 and 7 should be obtained regardless of which aspect of performance is stabilized on a moment-by-moment basis as required by the task or situational context.

Multiplicity of function in the basal ganglia and cerebellum

Within the feature space that we defined, the location of many ROIs lie close to the boundary between clusters 1 and 2, indicating that they share some similarity with both group response characteristics. Thus these regions might be expected to exhibit mixed activities, being generally elevated during stabilization with limited sensitivity to load type and passive movement. Indeed, activities in some cluster 2 regions close to the classification boundary correlated strongly with state estimation errors on a TR-by-TR basis (a pattern we consider a hallmark of optimal feedback regulatory behavior). There are sound anatomical and neurophysiological reasons why the boundary between clusters in our feature space might not be distinct. For example, some regions (e.g., the basal ganglia and the dentate nucleus of the cerebellum) project to multiple brain regions and may subserve a diversity of functions. Retrograde virus tracing studies have shown that the output projections of the basal ganglia reach multiple cortical areas implicated in the control of both motor and cognitive functions (Hoover and Strick 1993, 1999; Middleton and Strick 2000, 2002). Due to this plurality of output projections, it is not surprising that the basal ganglia have variously been implicated in many tasks such as movement selection based on the task context (Jueptner and Weiller 1998), the triggering of discrete motor actions (Rao et al. 1997; Taniwaki et al. 2003), optimizing of control policies to maximize future reward (Doya 2000), the optimization of feedback control parameters (Horak et al. 1992), the learning and encoding of movement sequences (Jueptner and Weiller 1998; Lehericy et al. 2005; Mushiake and Strick 1995) as well as in the regulation of wrist posture (Marsden 1982) via prolonged antagonist muscle co-contractions at the wrist (Mink and Thach 1991). This last function might explain the increased Δ_M observed in the basal ganglia because wrist muscle co-activation (but not excess activation) was greater in RT than CT stabilization periods.

Similarly, retrograde virus tracing studies have shown that the cerebellum also projects to multiple cortical areas through the dentate nucleus (Dum and Strick 2003; Kelly and Strick 2003; Middleton and Strick 2000). Both motor and cognitive areas are represented, consistent with reported cerebellar involvement in the ongoing control of motor tasks (e.g., visually guided movement; Mushiake and Strick 1993; Strick 1983) as well as in more cognitive functions (e.g., language, problem solving, sensory discrimination) (Gao et al. 1996; Kim et al. 1994; see Leiner et al. 1991 for a review). Future studies integrating robotic tools, immersive multisensory feedback environments and neural recording techniques may provide a means to disambiguate the cerebellum's contributions to sensory information processing and motor command updating in the control of limb posture and movement.

Conclusions

Using a novel combination of robotic and functional MR imaging techniques, we have found that subjects invoke multiple compensatory strategies during wrist stabilization against external perturbations without visual feedback. Our imaging data are consistent with the idea that distinct cortical-subcortical loops contribute to the optimal feedback control of limb position (cluster 1) and the feed-forward planning and execution of internally generated corrective movements (cluster 2). Specifically, we showed that distinct neural mechanisms contribute to the processing of kinematic errors over different time scales, one contributing to the on-line (moment-by-moment) control of limb posture and the other contributing to the adjustment of behavioral goals with a longer temporal integration period. These results highlight the importance of both postural and trajectory control mechanisms in peripheral limb stabilization. Additional studies are needed to better understand how the brain combines the different control processes to minimize performance errors (the value assignment problem) and how the brain arrives at computational solutions to various aspects of limb stabilization and movement control, including: multisensory integration for optimal state estimation, feedback optimization using adaptive internal models, and the context-dependent triggering of discrete corrections.

APPENDIX

Robot MR-compatibility testing

A series of tests were performed to validate the simultaneous acquisition of manipulandum data and scanner images both within a 1.5T GE Signa and a 3.0T GE Excite HD MR scanner (General Electric Healthcare, Milwaukee, WI), both located at Froedert Memorial Lutheran Hospital in Milwaukee, WI. Only the results of the 3.0T testing are presented in the following text because similar performance results were obtained in the 1.5T testing and because the 3.0T testing data permitted evaluation of potential MR signal phase distortion induced by the robot. A 3.0T spherical head phantom (GE Model No. 2359877) was supported within a split transmit/receive quadrature head coil (GE Model No. 2376114) and imaged during validation testing (Fig. A1*A*). An echo planar imaging pulse sequence (29 contiguous sagittal 6 mm slices; TE = 25 ms, TR = 2 s, Flip = 77°, FOV = 24 cm, and 4 × 4-mm in-plane resolution) was used to verify that operation of the manipulandum during scanning does not induce significant artifacts in functional MR images and to verify that the device could measure both pressure and joint angle without noise contamination during echo planar imaging.

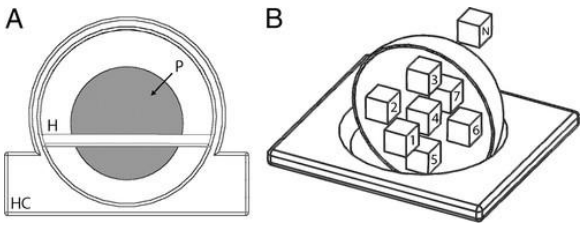

FIG. A1.*A*: illustration of the setup used to validate the MR compatibility of the robotic device: head coil (HC), phantom holder (H), and phantom (P). *B*: drawing of holder and phantom (cut away to show details of validation ROIs) including the ROIs used in the calculations of SNR and field homogeneity.

Validation testing used a blocked experimental design (duration = 270 s) such that during “activity” states, the computer controller cycled the device's handle through a sinusoidal trajectory (0.25 cycle/s), whereas the device remained motionless during “rest” states (50% duty cycle; period = 60 s). Complex k-space data (I and Q channel) were collected from the MR system during phantom imaging to allow for analysis of both magnitude and phase MR images. We quantified the effects of simultaneous operation of the robot and scanner by imaging the phantom with the robot at six distances: 0.25, 0.50, 0.75, 1.0, and 1.25 m from the center of the imaging volume as well as outside the scanning suite (∞). The phantom was sampled using seven equal volume ROIs

distributed within its spherical boundary to test whether operating the robot induces spatial anisotropies in the magnitude and phase images during scanning (Fig. A1*B*, 1–7).

We used two measures to evaluate MR signal quality during robot operation. First, we calculated the signal to noise ratio (SNR) within each ROI from the magnitude images

$$\mathrm{SNR_{ROI}} = \frac{\mu \mathrm{ROI}}{0.665 * \sigma_{\mathrm{noise}}}$$

where μ_{ROI} is the time series average within a given ROI and σ_{noise} is an estimate of noise in the magnitude images obtained by calculating the SD of the time series in an identically sized ROI located outside of the volume of the phantom (Fig A1*B*, N). The scaling factor 0.665 was used to correct for changes in the statistical distribution of σ_{noise} caused by the calculation of the magnitude image from the original complex MR data (Haacke et al. 1999). To quantify imaging artifacts induced by robot operation, two-way ANOVA and post hoc Tukey *t*-tests were used to compare SNR values at each distance and ROI with those obtained in the baseline condition, i.e., when the robot was outside the scanner suite (∞, Fig. A2*A*). Second, we use the phase images to quantify changes in magnetic field homogeneity induced by robot operation within the scanner suite. The average change in field homogeneity from baseline for each ROI (ΔB_{ROI}) was calculated (Haacke et al. 1999)

$$\Delta B_{\mathrm{ROI}} = \frac{\phi \mathrm{ROI}}{-\gamma \mathrm{T_E}}$$

where, ϕ_{ROI} is the average change in each ROI's phase time series with respect to baseline, γ is the gyromagnetic ratio, and T_E is the minimum full echo time of the EPI pulse sequence.

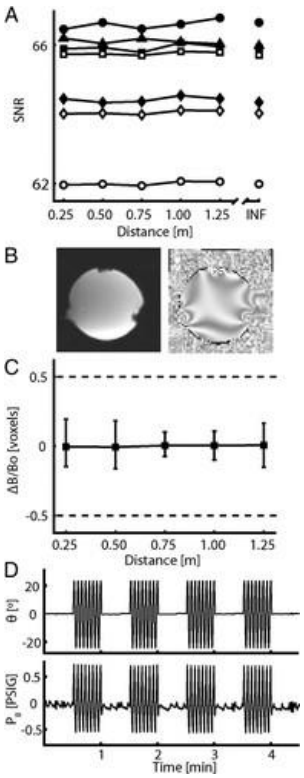

FIG. A2.*A*: signal-to-noise ratio (SNR) vs. distance of the device from the center of imaging volume for individual ROIs identified in Fig. A1*B.* SNR measurements were derived from magnitude images and did not vary significantly within each ROI across robot placement distances, demonstrating that robot operation had little effect on scanner performance. ROI 6 had the lowest SNR due to imaging ring artifact pictured in *B. B*: sagittal

slice of the EPI magnitude (*left*) and phase (*right*) images of the phantom. Notice the susceptibility artifact bilaterally in the lower portion of the image caused by the presence of the phantom holder. This artifact was seen in images both with and without the manipulandum in the scanner. *C*: estimate of field homogeneity in ROI 2 from collected phase data. All values of DeltaB/Bo were within expected ranges of field uniformity. *D*: measurements of wrist angle and bellows pressure taken during the validation experiment when the device was 0.50 m from the imaging volume. Pressure and volume measurements were not adversely effected by the operation of the MR scanner.

Finally, we quantified the effects of echo planar imaging on robot operation by calculating SNR for actuator pressure (SNR_P) and wrist angle (SNR_A) signals

$$\mathrm{SNR}_{\mathrm{P\ or\ A}} = 20 * \log_{10}\left(\frac{\mathrm{RMS}_{\mathrm{Signal}} - \mathrm{RMS}_{\mathrm{Noise}}}{\mathrm{RMS}_{\mathrm{Noise}}}\right)$$

Root mean squared (RMS) values of actuator pressure and joint angle were calculated during “activity” and “rest” states to approximate signal and noise, respectively.

Compatibility testing results

We computed the change in SNR within the seven phantom ROIs relative to the baseline (∞) condition caused by introducing the robot at five distances from the center of the imaging volume (Fig. A2*A*). Values of SNR varied across the seven ROIs but were relatively insensitive to robot placement distance within each individual ROI. ANOVA found main effects of both ROI [$F(6,30) = 3224.97$, $P < 0.0005$] and distance [$F(5,30) = 3.31$, $P < 0.017$], but comparison of SNR at the five distance treatments relative to baseline revealed no systematic change in SNR as a function of robot distance from the imaging volume ($P = 0.31$, 0.13, 0.97, 0.99, and 0.99 for distances 1.25, 1.0, 0.75, 0.5, and 0.25 m, respectively). The significant main effect of distance is due to an apparent *increase* in SNR at 1.0 m compared with SNR at 0.75 m ($P = 0.03$). The variation in SNR within the phantom volume with respect to ROI was clearly caused by local field artifacts induced by the phantom holder (Fig. A1*B*, H) and boundary effects at the phantom's outer shell (Fig. A2*B*) because these effects were observed when the robot was not present (∞, Fig. A2*A*).

Next, we computed the field distortion (ΔB/Bo) induced by the presence of the robot at each distance. As shown for a representative ROI (Fig. A1*C*, ROI 1), field inhomogeneity induced by the robot (ΔB/Bo) was well <0.5 voxels at each distance (Fig. A2*C*). A one-sided *t*-test rejected the null hypothesis that the average magnitude of the field distortion exceeded 0.5 voxel ($T_{35} = 239.7$, $P < 0.0005$), thus the BOLD response is not influenced by the device and its operation. Scanner operation also had minimal effects on manipulandum operation (Fig. A2*D*). Neither joint angle nor pressure SNR varied systematically as a function of distance. No difference was observed in measurements of SNR_{Angle} ($T_9 = 0.09$, $P = 0.934$) or $SNR_{Pressure}$ ($T_9 = 0.39$, $P = 0.705$) when compared with baseline measures (robot outside scanner environment). Performance of neither the scanner nor the robot is adversely influenced by operation of the robot during MR scanning. Similar performance results were obtained (and identical conclusions drawn) from testing conducted in the 1.5T GE Signa MR Scanner.

GRANTS

This work was supported by National Science Foundation Grant BES0238442, Division of Research Resources Grant NCRR GCRC M01-RR00058, and the Alvin W. and Marion Birnschein Foundation.

FOOTNOTES

- The costs of publication of this article were defrayed in part by the payment of page charges. The article must therefore be hereby marked "*advertisement*" in accordance with 18 U.S.C. Section 1734 solely to indicate this fact.

We thank J. Goldstein for crafting the manipulandum and Dr. N. Bansal for helpful suggestions regarding the statistical handling of the data as well as Dr. V. Roopchansingh, M. Verber and the MCW MRI technicians for assistance during fMRI data collection and analysis.

AUTHOR NOTES

- Address for reprint requests and other correspondence: R. A. Scheidt, Dept. of Biomedical Engineering, Olin Engineering Center, 303, P.O. Box 1881, Marquette University, Milwaukee, WI 53201-1881 (E-mail: scheidt@ieee.org)

REFERENCES

Box et al. 1994 Box GEP**, Jenkins GM, Reinsel GC.** ***Time Series Analysis: Forecasting and Control.*** Englewood Cliffs, NJ: Prentice Hall, 1994.

Brinkman and Porter 1979 Brinkman C**, Porter R.** Supplementary motor area in the monkey: activity of neurons during performance of a learned motor task. ***J Neurophysiol*** *42*: 681–709, 1979.

Buneo et al. 2002 Buneo CA**, Jarvis MR, Batista AP, Andersen RA.** Direct visuomotor transformations for reaching. ***Nature*** *416*: 632–636, 2002.

Carel et al. 2000 Carel C**, Loubinoux I, Boulanouar K, Manelfe C, Rascol O, Celsis P, Chollet F.** Neural substrate for the effects of passive training on sensorimotor cortical representation: a study with functional magnetic resonance imaging in healthy subjects. ***J Cereb Blood Flow Metab*** *20*: 478–484, 2000.

Carter et al. 1998 Carter CS**, Braver TS, Barch DM, Botvinick MM, Noll D, Cohen JD.** Anterior cingulate cortex, error detection, and the online monitoring of performance. ***Science*** *280*: 747–749, 1998.

Cox 1996 Cox RW**.** AFNI software for analysis and visualization of functional magnetic resonance neuroimages. ***Comput Biomed Res*** *29*: 162–173, 1996.

Dai et al. 2001 Dai TH**, Liu JZ, Sahgal V, Brown RW, Yue GH.** Relationship between muscle output and functional MRI-measured brain activation. ***Exp Brain Res*** *140*: 290–300, 2001.

Deiber et al. 1997 Deiber MP**, Wise SP, Honda M, Catalan MJ, Grafman J, Hallett M.** Frontal and parietal networks for conditional motor learning: a positron emission tomography study. ***J Neurophysiol*** *78*: 977–991, 1997.

Della-Maggiore et al. 2004 Della-Maggiore V**, Malfait N, Ostry DJ, Paus T.** Stimulation of the posterior parietal cortex interferes with arm trajectory adjustments during the learning of new dynamics. ***J Neurosci*** *24*: 9971–9976, 2004.

Desmurget et al. 1999 Desmurget M**, Epstein CM, Turner RS, Prablanc C, Alexander GE, Grafton ST.** Role of the posterior parietal cortex in updating reaching movements to a visual target. ***Nat Neurosci*** *2*: 563–567, 1999.

Desmurget et al. 2004 Desmurget M**, Grafton ST, Vindras P, Grea H, Turner RS.** The basal ganglia network mediates the planning of movement amplitude. ***Eur J Neurosci*** *19*: 2871–2880, 2004.

Desmurget et al. 2001 Desmurget M**, Grea H, Grethe JS, Prablanc C, Alexander GE, Grafton ST.** Functional anatomy of nonvisual feedback loops during reaching: a positron emission tomography study. ***J Neurosci*** *21*: 2919–2928, 2001.

Diedrichsen et al. 2005 Diedrichsen J**, Hashambhoy Y, Rane T, Shadmehr R.** Neural correlates of reach errors. ***J Neurosci*** *25*: 9919–9931, 2005.

Doya 2000 Doya K**.** Complementary roles of basal ganglia and cerebellum in learning and motor control. ***Curr Opin Neurobiol*** *10*: 732–739, 2000.

Dum and Strick 2003 Dum RP**, Strick PL.** An unfolded map of the cerebellar dentate nucleus and its projections to the cerebral cortex. ***J Neurophysiol*** *89*: 634–639, 2003.

Ehrsson et al. 2001 Ehrsson HH**, Fagergren E, Forssberg H.** Differential fronto-parietal activation depending on force used in a precision grip task: an fMRI study. ***J Neurophysiol*** *85*: 2613–2623, 2001.

Evarts and Fromm 1981 Evarts EV**, Fromm C.** Transcortical reflexes and servo control of movement. ***Can J Physiol Pharmacol*** *59*: 757–775, 1981.

Evarts and Tanji 1976 Evarts EV**, Tanji J.** Reflex and intended responses in motor cortex pyramidal tract neurons of monkey. ***J Neurophysiol*** *39*: 1069–1080, 1976.

Evarts and Vaughn 1978 Evarts EV**, Vaughn WJ.** Intended arm movements in response to externally produced arm displacements in man. In: ***Cerebral Motor Control in Man: Long Loop Mechanisms***, edited by Desmedt JE. Basel: Karger, 1978, p. 178–192.

Fagg et al. 1998 Fagg AH**, Barto AG, Houk JC.** Learning to reach via corrective movements. In: ***Proc 10th Yale Workshop Adapt and Learning Syst.*** New Haven, CT: Yale, 1998, p. 179–185.

Fetz et al. 1980 Fetz EE**, Finocchio DV, Baker MA, Soso MJ.** Sensory and motor responses of precentral cortex cells during comparable passive and active joint movements. ***J Neurophysiol*** *43*: 1070–1089, 1980.

Flament et al. 1996 Flament D**, Ellermann JM, Kim SG, Ugurbil K, Ebner TJ.** Functional magnetic resonance imaging of cerebellar activation during the learning of a visuomotor dissociation task. ***Hum Brain Map*** *4*: 210–226, 1996.

Gao et al. 1996 Gao JH**, Parsons LM, Bower JM, Xiong J, Li J, Fox PT.** Cerebellum implicated in sensory acquisition and discrimination rather than motor control. ***Science*** *272*: 545–547, 1996.

Ghez et al. 2004 Ghez C**, Dinstein I, Cappell J, Scheidt RA.** Posture and movement are encoded in different coordinate systems. ***Soc Neurosci Abstr*** *873.13*, 2004.

Goldman-Rakic 1987 Goldman-Rakic PS**.** Motor control function of the prefrontal cortex. ***Ciba Found Symp*** *132*: 187–200, 1987.

Gomi and Osu 1998 Gomi H**, Osu R.** Task-dependent viscoelasticity of human multijoint arm and its spatial characteristics for interaction with environments. ***J Neurosci*** *18*: 8965–8978, 1998.

Grafton et al. 1998 Grafton ST**, Fagg AH, Arbib MA.** Dorsal premotor cortex and conditional movement selection: a PET functional mapping study. ***J Neurophysiol*** *79*: 1092–1097, 1998.

Haacke et al. 1999 Haacke EM**, Brown RW, Thompson MR, Venkatesan R.** ***Magnetic Resonance Imaging: Physical Principles and Sequence Design.*** New York: Wiley, 1999.

Haaland and Harrington 1989 Haaland KY**, Harrington DL.** Hemispheric control of the initial and corrective components of aiming movements. ***Neuropsychologia*** *27*: 961–969, 1989.

Hogan 1985 Hogan N**.** The mechanics of multi-joint posture and movement control. ***Biol Cybern*** *52*: 315–331, 1985.

Hoover and Strick 1993 Hoover JE**, Strick PL.** Multiple output channels in the basal ganglia. ***Science*** *259*: 819–821, 1993.

Hoover and Strick 1999 Hoover JE**, Strick PL.** The organization of cerebellar and basal ganglia outputs to primary motor cortex as revealed by retrograde transneuronal transport of herpes simplex virus type 1. ***J Neurosci*** *19*: 1446–1463, 1999.

Horak et al. 1992 Horak FB**, Nutt JG, Nashner LM.** Postural inflexibility in parkinsonian subjects. ***J Neurol Sci*** *111*: 46–58, 1992.

Horne and Butler 1995 Horne MK**, Butler EG.** The role of the cerebello-thalamo-cortical pathway in skilled movement. ***Prog Neurobiol*** *46*: 199–213, 1995.

Imamizu et al. 2000 Imamizu H**, Miyauchi S, Tamada T, Sasaki Y, Takino R, Putz B, Yoshioka T, Kawato M.** Human cerebellar activity reflecting an acquired internal model of a new tool. ***Nature*** *403*: 192–195, 2000.

Jahanshahi et al. 1995 Jahanshahi M**, Jenkins IH, Brown RG, Marsden CD, Passingham RE, Brooks DJ.** Self-initiated versus externally triggered movements. I. An investigation using measurement of regional cerebral blood flow with PET and movement-related potentials in normal and Parkinson's disease subjects. ***Brain*** *118*: 913–933, 1995.

Johnson and Wichern 2002 Johnson RA**, Wichern DW.** ***Applied Multivariate Statistical Analysis.*** Upper Saddle River, NJ: Prentice Hall, 2002.

Jueptner et al. 1997 Jueptner M**, Ottinger S, Fellows SJ, Adamschewski J, Flerich L, Muller SP, Diener HC, Thilmann AF, Weiller C.** The relevance of sensory input for the cerebellar control of movements. ***Neuroimage*** *5*: 41–48, 1997.

Jueptner and Weiller 1998 Jueptner M**, Weiller C.** A review of differences between basal ganglia and cerebellar control of movements as revealed by functional imaging studies. ***Brain*** *121*: 1437–1449, 1998.

Kawato and Gomi 1992 Kawato M**, Gomi H.** A computational model of four regions of the cerebellum based on feedback-error learning. ***Biol Cybern*** *68*: 95–103, 1992.

Kelly and Strick 2003 Kelly RM**, Strick PL.** Cerebellar loops with motor cortex and prefrontal cortex of a non-human primate. ***J Neurosci*** *23*: 8432–8444, 2003.

Kim et al. 1994 Kim SG**, Ugurbil K, Strick PL.** Activation of a cerebellar output nucleus during cognitive processing. ***Science*** *265*: 949–951, 1994.

Kitazawa et al. 1998 Kitazawa S**, Kimura T, Yin PB.** Cerebellar complex spikes encode both destinations and errors in arm movements. ***Nature*** *392*: 494–497, 1998.

Kurtzer et al. 2005 Kurtzer I**, Herter TM, Scott SH.** Random change in cortical load representation suggests distinct control of posture and movement. ***Nat Neurosci*** *8*: 498–504, 2005.

Lackner and Dizio 1994 Lackner JR**, Dizio P.** Rapid adaptation to Coriolis force perturbations of arm trajectory. ***J Neurophysiol*** *72*: 299–313, 1994.

Lacquaniti et al. 1993 Lacquaniti F**, Carrozzo M, Borghese NA.** Time-varying mechanical behavior of multijointed arm in man. ***J Neurophysiol*** *69*: 1443–1464, 1993.

Lee and Tatton 1975 Lee RG**, Tatton WG.** Motor responses to sudden limb displacements in primates with specific CNS lesions and in human patients with motor system disorders. ***Can J Neurol Sci*** *2*: 285–293, 1975.

Lehericy et al. 2005 Lehericy S**, Benali H, Van de Moortele PF, Pelegrini-Issac M, Waechter T, Ugurbil K, Doyon J.** Distinct basal ganglia territories are engaged in early and advanced motor sequence learning. ***Proc Nat Acad Sci USA*** *102*: 12566–12571, 2005.

Leiner et al. 1991 Leiner HC**, Leiner AL, Dow RS.** The human cerebro-cerebellar system: its computing, cognitive, and language skills. ***Behav Brain Res*** *44*: 113–128, 1991.

Loeb et al. 1999 Loeb GE**, Brown IE, Cheng EJ.** A hierarchical foundation for models of sensorimotor control. ***Exp Brain Res*** *126*: 1–18, 1999.

Marsden 1982 Marsden CD**.** The mysterious motor function of the basal ganglia: the Robert Wartenberg Lecture. ***Neurology*** *32*: 514–539, 1982.

Marsden et al. 1972 Marsden CD**, Merton PA, Morton HB.** Servo action in human voluntary movement. ***Nature*** *238*: 140–143, 1972.

Marsden et al. 1978 Marsden CD**, Merton PA, Morton HB, Adam JER, Hallett M.** Automatic and Voluntary Responses to Muscle Stretch in Man. In: ***Cerebral Motor Control in Man: Long Loop Mechanisms***, edited by Desmedt JE. Basel; New York: Karger, 1978, p. 167–177.

Matthews 1981 Matthews PBC**.** Muscle spindles their messages and their fusimotor supply. In: ***Handbook of Physiology. The Nervous System. Motor Control***, edited by Brookhart JM, Mountcastle VB, Brooks VB. Bethesda, MD: Am. Physiol. Soc., 1981, sect. 1, vol. II, p. 189–228.

Miall et al. 2000 Miall RC**, Imamizu H, Miyauchi S.** Activation of the cerebellum in co-ordinated eye and hand tracking movements: an fMRI study. ***Exp Brain Res*** *135*: 22–33, 2000.

Miall et al. 2001 Miall RC**, Reckess GZ, Imamizu H.** The cerebellum coordinates eye and hand tracking movements. ***Nat Neurosci*** *4*: 638–644, 2001.

Miall et al. 1993 Miall RC**, Weir DJ, Wolpert DM, Stein JF.** Is the cerebellum a Smith predictor? ***J Mot Behav*** *25*: 203–216, 1993.

Middleton and Strick 2000 Middleton FA**, Strick PL.** Basal ganglia output and cognition: evidence from anatomical, behavioral, and clinical studies. ***Brain Cogn*** *42*: 183–200, 2000.

Middleton and Strick 2002 Middleton FA**, Strick PL.** Basal-ganglia "projections" to the prefrontal cortex of the primate. ***Cereb Cortex*** *12*: 926–935, 2002.

Milner 2002 Milner TE**.** Adaptation to destabilizing dynamics by means of muscle cocontraction. ***Exp Brain Res*** *143*: 406–416, 2002.

Mima et al. 1999 Mima T**, Sadato N, Yazawa S, Hanakawa T, Fukuyama H, Yonekura Y, Shibasaki H.** Brain structures related to active and passive finger movements in man. ***Brain*** *122*: 1989–1997, 1999.

Mink and Thach 1991 Mink JW**, Thach WT.** Basal ganglia motor control. III. Pallidal ablation: normal reaction time, muscle cocontraction, and slow movement. ***J Neurophysiol*** *65*: 330–351, 1991.

Mushiake and Strick 1993 Mushiake H**, Strick PL.** Preferential activity of dentate neurons during limb movements guided by vision. ***J Neurophysiol*** *70*: 2660–2664, 1993.

Mushiake and Strick 1995 Mushiake H**, Strick PL.** Pallidal neuron activity during sequential arm movements. ***J Neurophysiol*** *74*: 2754–2758, 1995.

Mussa-Ivaldi et al. 1985 Mussa-Ivaldi FA**, Hogan N, Bizzi E.** Neural, mechanical, and geometric factors subserving arm posture in humans. ***J Neurosci*** *5*: 2732–2743, 1985.

Neilson 1972 Neilson PD**.** Interaction between voluntary contraction and tonic stretch reflex transmission in normal and spastic patients. ***J Neurol Neurosurg Psych*** *35*: 853–860, 1972.

Nezafat et al. 2001 Nezafat R**, Shadmehr R, Holcomb HH.** Long-term adaptation to dynamics of reaching movements: a PET study. ***Exp Brain Res*** *140*: 66–76, 2001.

Nichols and Houk 1976 Nichols TR**, Houk JC.** Improvement in linearity and regulation of stiffness that results from actions of stretch reflex. ***J Neurophysiol*** *39*: 119–142, 1976.

Norris et al. 2004 Norris SA**, Greger B, Hathaway EN, Thach WT.** Purkinje cell spike firing in the posterolateral cerebellum: correlation with visual stimulus, oculomotor response, and error feedback. ***J Neurophysiol*** *92*: 1867–1879, 2004.

Oldfield 1971 Oldfield RC**.** The assessment and analysis of handedness: the Edinburgh inventory. ***Neuropsychology*** *9*: 97–113, 1971.

Picard and Strick 2001 Picard N**, Strick PL.** Imaging the premotor areas. ***Curr Opin Neurobiol*** *11*: 663–672, 2001.

Pisella et al. 2000 Pisella L**, Grea H, Tilikete C, Vighetto A, Desmurget M, Rode G, Boisson D, Rossetti Y.** An "automatic pilot" for the hand in human posterior parietal cortex: toward reinterpreting optic ataxia. ***Nat Neurosci*** *3*: 729–736, 2000.

Porter and Lemon 1995 Porter R**, Lemon R.** ***Corticospinal Function and Voluntary Movement.*** Oxford, UK: Clarendon, 1995.

Rack 1981 Rack PM**.** Limitations of somatosensory feedback control in posture and movement. In: ***Handbook of Physiology. The Nervous System. Motor Control***, edited by Brookhart JM, Mountcastle VB, Brooks VB. Bethesda: Am. Physiol. Soc, 1981, sect. 1, vol. II, p. 229–256.

Rao et al. 1997 Rao SM**, Harrington DL, Haaland KY, Bobholz JA, Cox RW, Binder JR.** Distributed neural systems underlying the timing of movements. ***J Neurosci*** *17*: 5528–5535, 1997.

Rubia et al. 2001 Rubia K**, Russell T, Overmeyer S, Brammer MJ, Bullmore ET, Sharma T, Simmons A, Williams SC, Giampietro V, Andrew CM, Taylor E.** Mapping motor inhibition: conjunctive brain activations across different versions of go/no-go and stop tasks. ***Neuroimage*** *13*: 250–261, 2001.

Sakai et al. 1999 Sakai K**, Hikosaka O, Miyauchi S, Sasaki Y, Fujimaki N, Putz B.** Presupplementary motor area activation during sequence learning reflects visuo-motor association (Rapid Communication). ***J Neurosci*** *19*: 1, 1999.

Scheidt et al. 2004 Scheidt RA**, Mussa-Ivaldi FA, Ghez C.** Posture and movement invoke separate adaptive mechanisms. ***Soc Neurosci Abstr*** 873.14, 2004.

Schmahmann 2000 Schmahmann JD**.** ***MRI Atlas of the Human Cerebellum.*** San Diego: Academic, 2000.

Scott 2004 Scott SH**.** Optimal feedback control and the neural basis of volitional motor control. ***Nat Rev Neurosci*** *5*: 532–546, 2004.

Scott and Kalaska 1997 Scott SH**, Kalaska JF.** Reaching movements with similar hand paths but different arm orientations. I. Activity of individual cells in motor cortex. ***J Neurophysiol*** *77*: 826–852, 1997.

Scott et al. 1997 Scott SH**, Sergio LE, Kalaska JF.** Reaching movements with similar hand paths but different arm orientations. II. Activity of individual cells in dorsal premotor cortex and parietal area 5. ***J Neurophysiol*** *78*: 2413–2426, 1997.

Seidler et al. 2004 Seidler RD**, Noll DC, Thiers G.** Feedforward and feedback processes in motor control. ***Neuroimage*** *22*: 1775–1783, 2004.

Shadmehr and Holcomb 1997 Shadmehr R**, Holcomb HH.** Neural correlates of motor memory consolidation. ***Science*** *277*: 821–825, 1997.

Shen and Alexander 1997 Shen L**, Alexander GE.** Preferential representation of instructed target location versus limb trajectory in dorsal premotor area. ***J Neurophysiol*** *77*: 1195–1212, 1997.

Sinkjaer et al. 2000 Sinkjaer T**, Andersen JB, Ladouceur M, Christensen LO, Nielsen JB.** Major role for sensory feedback in soleus EMG activity in the stance phase of walking in man. ***J Physiol 523 Pt*** *3*: 817–827, 2000.

Sinkjaer and Hayashi 1989 Sinkjaer T**, Hayashi R.** Regulation of wrist stiffness by the stretch reflex. ***J Biomech*** *22*: 1133–1140, 1989.

Smeets et al. 2005 Smeets JBJ**, van den Dobbelsteen JJ, van Beers RJ, Brenner E.** Movement drift is the result of optimal sensory combination. In: ***Adv Comp Mot Contr IV.*** Washington DC: 2005.

Soso and Fetz 1980 Soso MJ**, Fetz EE.** Responses of identified cells in postcentral cortex of awake monkeys during comparable active and passive joint movements. ***J Neurophysiol*** *43*: 1090–1110, 1980.

Strick 1978 Strick PL**.** Cerebellar Involvement in volitional muscle responses to load changes. In: ***Cerebral Motor Control in Man: Long Loop Mechanisms***, edited by Desmedt JE. Basel: Karger, 1978, p. 85–93.

Strick 1983 Strick PL**.** The influence of motor preparation on the response of cerebellar neurons to limb displacements. ***J Neurosci*** *3*: 2007–2020, 1983.

Suminski and Scheidt 2004 Suminski AJ**, Scheidt RA.** Control System for MRI-compatible pneumatic manipulandum. ***Proc BMES*** 1143, 2004.

Talairach and Tournoux 1988 Talairach J**, Tournoux P.** ***Co-Planar Stereotaxic Atlas of the Human Brain.*** Stuttgart: Thieme, 1988.

Taniwaki et al. 2003 Taniwaki T**, Okayama A, Yoshiura T, Nakamura Y, Goto Y, Kira J, Tobimatsu S.** Reappraisal of the motor role of basal ganglia: a functional magnetic resonance image study. ***J Neurosci*** *23*: 3432–3438, 2003.

Tanji and Kurata 1979 Tanji J**, Kurata K.** Neuronal activity in the cortical supplementary motor area related with distal and proximal forelimb movements. ***Neurosci Lett*** *12*: 201–206, 1979.

Thach 1978 Thach WT**.** Correlation of neural discharge with pattern and force of muscular activity, joint position, and direction of intended next movement in motor cortex and cerebellum. ***J Neurophysiol*** *41*: 654–676, 1978.

Thickbroom et al. 1998 Thickbroom GW**, Phillips BA, Morris I, Byrnes ML, Mastaglia FL.** Isometric force-related activity in sensorimotor cortex measured with functional MRI. ***Exp Brain Res*** *121*: 59–64, 1998.

Thoroughman and Shadmehr 1999 Thoroughman KA**, Shadmehr R.** Electromyographic correlates of learning an internal model of reaching movements. ***J Neurosci*** *19*: 8573–8588, 1999.

Todorov and Jordan 2002 Todorov E**, Jordan MI.** Optimal feedback control as a theory of motor coordination. ***Nat Neurosci*** *5*: 1226–1235, 2002.

Tunik et al. 2005 Tunik E**, Frey SH, Grafton ST.** Virtual lesions of the anterior intraparietal area disrupt goal-dependent on-line adjustments of grasp. ***Nat Neurosci*** *8*: 505–511, 2005.

Vaillancourt et al. 2003 Vaillancourt DE**, Thulborn KR, Corcos DM.** Neural basis for the processes that underlie visually guided and internally guided force control in humans. ***J Neurophysiol*** *90*: 3330–3340, 2003.

Van Essen et al. 2001 Van Essen DC**, Drury HA, Dickson J, Harwell J, Hanlon D, Anderson CH.** An integrated software suite for surface-based analyses of cerebral cortex. ***J Am Med Inform Assoc*** *8*: 443–459, 2001.

Weiller et al. 1996 Weiller C**, Juptner M, Fellows S, Rijntjes M, Leonhardt G, Kiebel S, Muller S, Diener HC, Thilmann AF.** Brain representation of active and passive movements. ***Neuroimage*** *4*: 105–110, 1996.

Widrow and Walach 1996 Widrow B**, Walach E.** ***Adaptive Inverse Control.*** Upper Saddle River, NJ: Prentice Hall, 1996.

Winstein et al. 1997 Winstein CJ**, Grafton ST, Pohl PS.** Motor task difficulty and brain activity: investigation of goal-directed reciprocal aiming using positron emission tomography. ***J Neurophysiol*** *77*: 1581–1594, 1997.

Wolpert and Flanagan 2001 Wolpert DM**, Flanagan JR.** Motor prediction. ***Curr Biol*** *11*: R729–732, 2001.

Wolpert et al. 1998 Wolpert DM**, Goodbody SJ, Husain M.** Maintaining internal representations: the role of the human superior parietal lobe. ***Nat Neurosci*** *1*: 529–533, 1998.

Wong et al. 1978 Wong YC**, Kwan HC, MacKay WA, Murphy JT.** Spatial organization of precentral cortex in awake primates. I. Somatosensory inputs. ***J Neurophysiol*** *41*: 1107–1119, 1978.